Distinct Neuropeptide-Receptor Modules Regulate a Sex-Specific Behavioral Response to a Pheromone

Author Names and Affiliations:

Douglas K. Reilly[1,6], Emily J. McGlame[1,7], Elke Vandewyer[2], Annalise M. Robidoux[1,3], Haylea T. Northcott[1,4,8], William Joyce[5], Mark J. Alkema[5], Robert J. Gegear[9], Isabel Beets[2], Jagan Srinivasan[1,4,*]

[1] Department of Biology and Biotechnology, Worcester Polytechnic Institute, Worcester, MA 01605, USA

[2] Neural Signaling and Circuit Plasticity Group, Department of Biology, KU Leuven, Leuven, BEL

[3] Department of Chemistry and Biochemistry, Worcester Polytechnic Institute, Worcester, MA 01605, USA

[4] Program of Bioinformatics and Computational Biology, Worcester Polytechnic Institute, Worcester, MA 01605, USA

[5] Neurobiology Department, University of Massachusetts Medical School, Worcester, MA 01605, USA

[6] Present address: Tufts University, Medford, MA 02155, USA

[7] Present address: AbbVie Foundational Neuroscience Center, Cambridge, MA 02139, USA

[8] Present address: Optum, Hartford, CT 06103, USA

[9] Department of Biology, University of Massachusetts Dartmouth, Dartmouth, MA 02747, USA

* Corresponding author: Jagan Srinivasan, jsrinivasan@wpi.edu

Key words: *C. elegans*, Ascaroside, Pheromone, Behavioral Valence, Neuropeptide, Sex-specific

Abstract

Dioecious species are a hallmark of the animal kingdom, with opposing sexes responding differently to identical sensory cues. Here, we study the response of *C. elegans'* to the small-molecule pheromone, ascr#8, which elicits opposing behavioral valences in each sex. We identify a novel neuropeptide-neuropeptide receptor (NP/NPR) module that is active in males, but not in hermaphrodites. Using a novel paradigm of neuropeptide rescue that we established, we leverage bacterial expression of individual peptides to rescue the sex-specific response to ascr#8. Concurrent biochemical studies confirmed individual FLP-3 peptides differentially activate two divergent receptors, NPR-10 and FRPR-16. Interestingly, the two of the peptides that rescued behavior in our feeding paradigm are related through a conserved threonine, suggesting that a specific NP/NPR combination sets a male state, driving the correct behavioral valence of the ascr#8 response. Receptor expression within pre-motor neurons reveals novel coordination of male-specific and core locomotory circuitries.

Introduction

Sex-specific behaviors are unique aspects of survival throughout the animal kingdom from invertebrates to humans [1-3]. These behaviors include a wide range of coordinated and genetically pre-programmed social and sexual displays that ensure successful reproductive strategies, ultimately resulting in survival of the species in its natural environment [2,3]. The neural circuits regulating these behavioral responses are conserved, and often shared between sexes, but dependent on social experience and physiological state [2]. For example, the vomeronasal and main olfactory epithelium in mice are required for male aggression and mating, but in females they contribute towards receptivity and aggression [3]. Prominent among these stimuli are mating cues [4]; while the visual displays of higher order animals are among the most apparent of these, chemical mating cues are the most ubiquitous, with entire sensory organs dedicated to pheromone sensation [5].

Pheromones are small-molecule signals between conspecifics that convey information on the sender's current physiological state, and potentially life stage and developmental history [6,7]. How the nervous system responds to these stimuli is dependent on both the internal, physiological state of the animal [8], and external, concurrently sensed stimuli [9]. We have previously shown that behavioral response to pheromones is directly dependent on the physiological state of the animal [10], though the mechanisms which determine such responses remain enigmatic.

Nematodes communicate through a large and growing class of pheromones termed ascarosides (ascr) [6]. These small molecules convey social as well as developmental information, and the assays used to understand the roles of these cues have varied [4,6]. There are multiple ascarosides found to communicate attractive behaviors, specifically in a sex-specific manner, including: ascr#1, ascr#2, ascr#3, ascr#4, and ascr#8 [11]. Unique among ascaroside structures is

the presence of a *p*-aminobenzoate group – a folate precursor that *C. elegans* are unable to synthesize, yet obtain from bacterial food sources [12] – at the terminus of ascr#8. This pheromone has previously been shown to act as an extremely potent male attractant, being sensed via a chemosensory pathway shared with ascr#3: the male specific CEM neurons [13]. However, whereas ascr#3 is also sensed by over half a dozen chemosensory neurons [13-16], ascr#8 has only been shown to be sensed by the male-specific CEM [13].

While the CEMs offer a sex-specific mode of chemosensation for ascr#8, neuromodulators and hormones are heavily implicated in all stages of the sex-specific and pheromone-elicited *C. elegans* mating behaviors. Prior to sensation of mating cues, the mate searching behavior of male *C. elegans* is modulated by the neuropeptide, PDF-1 [17,18]. Interestingly, this neuropeptide also controls the sexual identity of the ASJ chemosensory neurons [19]. The mating pheromone ascr#3 is modulated by insulin signaling [20], while activation of ascr#3-sensing neurons also activates the NPR-1 receptor [16]. Finally, the physical act of male sexual turning during mating is mediated by multiple FMRFamide-like peptides [21]. This complex regulation of behaviors relies on specific neuropeptide-neuropeptide receptor (NP/NPR) modules.

Unique NP/NPR modules are known to drive specific physiological and behavioral responses in *C. elegans* [22]. While DAF-2 propagates insulin-like peptide (*ins*) signaling, the specific peptide determines the effect. For example, *ins-4* functions in learning, while *ins-6* affects synapse formation [23,24]. Meanwhile, avoidance of ascr#3 by hermaphrodites is mediated in part by INS-18/DAF-2 signaling – higher levels of *ins-18* expression result in lower ascr#3 avoidance rates [20]. Conversely, FMRFamide-like peptide (*flp*) genes, many of which encode multiple peptides, signal through a complex network in which multiple receptors sense identical peptides, and multiple FLP peptides activate the same receptors. For instance, activation of NPR-4 by

FLP-18 modulates reversal length [25], while the sensation of the divergent FLP-4 by the same receptor contributes to food preference choice [26].

Here, we investigate the neuronal mechanisms governing the behavioral attractive response of male *C. elegans* to ascr#8 [27]. Males exhibit a unique behavioral tuning curve to ascr#8, preferring concentrations in the 1 μM range, no longer being attracted to higher concentrations [13]. Given that multiple *flp* NP/NPR modules have been shown to play roles in setting physiological state [28], as well as linking sensation to physiology and behavior [29-31], we reasoned that peptidergic signaling is likely to play a role in the male ascr#8 behavioral response.

Previous studies of *C. elegans* behavioral responses to attractive social ascarosides employed a Spot Retention Assay (SRA) [13,32]. However, we found that the SRA contains several drawbacks, including male-male contact and the inability to track individual animals through the course of an assay. To address these issues, we have developed a single worm attraction assay (SWAA): a more robust assay that determines variables on a per-worm basis, and not solely at the population level. We utilized our novel SWAA to examine the responses of *him-8* males defective in *flp* neuropeptide genes expressed in male-specific neurons; *flp-3*, *flp-6*, *flp-12*, and *flp-19* [33]. In doing so, we discovered that *flp-3* plays a role in determining the sex-specific behavioral valence: i.e., determining whether the response to ascr#8 is attractive or aversive [15,34,35].

We identified two divergent FLP-3 receptors responsible for sensing the processed neuropeptides. Receptor activation studies elucidated that the previously identified *flp-3*-sensing G protein-coupled receptor, NPR-10 [22], and the novel FRPR-16, are both activated by FLP-3 peptides at nanomolar affinities. Additionally, loss-of-function mutations in either receptor result in behavioral defects that parallel those observed in *flp-3* mutants.

To more completely understand the role of *flp-3* in mediating the ascr#8 behavioral response, we adapted a peptide rescue-by-feeding protocol [36]. Using this method, we were able to rescue individual peptides in *flp-3* mutant animals and showed that a specific subset of FLP-3 peptides responsible for suppressing the avoidance differs from those responsible for driving male attraction to ascr#8.

Here we show that individual neuropeptides encoded by the *flp-3* gene exhibit specific biological activity, by binding multiple receptors, to drive the behavioral valence to a cue in a sex-specific manner.

Results

Spot Retention Assay vs. Single Worm Assay

We adapted the Spot Retention Assay (**Supp. Fig. 1**) [27,37] to allow for better characterization of individual worm behavior and robust interrogation of attraction to small molecules. We first compared the attractiveness of 1 μM ascr#8 (**Fig. 1A, inset**) across multiple strains of *C. elegans* (the wild-type N2 strain, the high incidence of male *him-5* and *him-8* strains, and the chemosensory cilia defective *osm-3*), using our novel behavioral assay, the single worm attraction assay (SWAA) (**Fig. 1A**). In this assay, individual animals are placed directly into the spot of the ascaroside cue while simultaneously removing any potential of male-male contact.

C. elegans exhibited a significant increase in the amount of time spent within ascr#8 spot compared to the vehicle control (**Fig. 1 B, C**), in all wild-type and *him* strains tested, in line with SRA results (**Supp. Fig. 1**). Normalized increase in dwell time, calculated as log(fold-change) [i.e., ascaroside dwell time over vehicle dwell time], allows for direct comparison between strains and conditions while accounting for baseline variability in vehicle dwell times. Using this

log(fold-change) metric, we can see that the increase in attraction to ascr#8 is consistent across N2, *him-5*, and *him-8* strains (**Fig. 1C**).

This assay also allows for measurement of the number of visits per worm (**Supp. Fig. 2A, C**), as well as the percentage of attractive visits to the cue, revealing no difference between any strain (**Supp. Fig. 2B**). Measuring attraction as of visits longer than two standard deviations above the mean vehicle dwell time, we show that males are indeed attracted to the cue itself, and not the male-male contact. These results also show that it is in fact a minority of animals (30%-45%) that exhibit attractive visits to the cue (**Supp. Fig. 2B**). This rate of behavioral attraction is consistent with calcium imaging experiments wherein ascr#8 exposure elicits similar rates of calcium transients in the CEM neurons [38].

Unlike the SRA, wherein hermaphrodites did not exhibit any difference in dwell time between vehicle and ascr#8 (**Supp. Fig. 1D, E**), our SWAA revealed that hermaphrodites from all strains consistently spent significantly less time in ascr#8 than the vehicle, with no difference between the spatial and vehicle control dwell times (**Fig. 2D,E**). Hermaphrodites also visited the ascaroside cue less than they did vehicle or spatial control well centers and exhibited little-to-no attractive visits (**Supp. Fig 2. C, D**).

Together, these data validate the SWAA as a robust assay for the measurement of the attractiveness of a cue on a single animal basis in both sexes. It also provides data on visit count and the percent of attractive visits that was previously impossible utilizing the SRA. Interestingly, attractive visits were only observed in 30%-45% of the time (**Supp. Fig. 2B**), suggesting that the individual state of the animal plays a critical role in determining the behavioral response to the ascaroside, as seen in other ascaroside behavioral responses [10,39].

Peptidergic Signaling Drives Sex-Specific ascr#8 Behavioral Response

Several neuropeptides of the FMRFamide-like-peptide (FLP) family have been implicated in the mechanosensory regulation of male-mating behavior [37]. The genes encoding the neuropeptides *flp-8*, *flp-10*, *flp-12*, and *flp-20* all suppress the number of turns around a hermaphrodite executed by a male prior to mating [21]. Despite this enrichment of *flp* genes functioning in the mechanosensation of these male specific behaviors [21], there has been no neuropeptide found to regulate the chemosensation of mating ascarosides. We sought to understand why an attractive concentration of a mating pheromone does not result in consistent attraction (**Supp. Fig. 2B**) by investigating potential peptidergic signaling pathways that function in the sensation of ascr#8.

We focused our initial screening of neuropeptides on the FLP family. We generated *him-8* lines of *flp* genes expressed in male-specific neurons, specifically *flp-3*, *flp-6*, *flp-12*, and *flp-19* [33]. To avoid confounding variables, our criteria for selection stipulated that outside of male-specific neurons, expression profiles would be limited to a small number of neurons (*flp-5* was therefore excluded as it exhibits expression in the pharyngeal muscle; while *flp-21* and *flp-22* are expressed in a large number of neurons outside of the male-specific expression profiles).

We found that loss of *flp-3* strongly affected the ability of male *C. elegans* to respond to ascr#8, (**Fig. 2A, B, Supp. Fig. 3A, B**). The log(fold-change) of *flp-3* is the only value significantly different than that seen in the wild-type (**Fig. 2B**). Interestingly, there was no defect seen in *flp-3* hermaphrodites, nor any other strain (**Fig 2D, E, Supp. Fig. 3C, D**).

Because the defect in male response to ascr#8 was significant, and the SWAA was designed to detect attractive behaviors, we sought to determine if *flp-3* loss-of-function (*lof*) animals were in fact avoiding ascr#8. Using a previously described drop avoidance assay [10,40], we exposed forward moving animals to a drop of either vehicle control or ascr#8 and scored the avoidance

index. Wild-type males did not avoid the cue, as expected for an attractive cue, while *flp-3 lof* males strongly avoided the pheromone (**Fig. 2C**). The hermaphroditic behavior was unaffected by the loss of *flp-3*. (**Fig. 2F**). Together, these results suggest that *flp-3* functions to control the behavioral valence of the ascr#8 response to be attractive in a sex-specific manner; serving in males to suppress a basal avoidance behavior observed in hermaphrodites.

Rescue of *flp-3* under a 4-kb region of its endogenous promoter was able to restore the behavioral valence of males to wild-type levels (**Fig. 2G-I, Supp. Fig. 3E, F**). While overexpression of neuropeptides can result in dominant negative phenotypes [17], expression of the *flp-3* construct in wild-type animals did not alter wild-type behavioral response to ascr#8 (**Fig.2G-I, Supp. Fig. 3E, F**).

To rule out an allele specific effect of the *flp-3(pk361)* mutation, which results in deletion of the entire coding sequence as well as 439 bp of upstream and 1493 bp of downstream genomic sequence [41], we also assayed *flp-3(ok3265)*, an in-frame deletion of the coding sequence that retains expression of two peptides produced by the *flp-3* gene [42] (FLP-3-1 and FLP-3-4) (**Supp. Fig. 4A**). The *flp-3(pk361) and flp-3(ok3265)* mutant phenotypes were identical (**Supp. Fig. 4B-F**), confirming that the deletion in the *pk361* allele did not cause any off-target effects, and that the two peptides encoded by the *ok3625* allele were not sufficient to rescue the mutant phenotype.

FLP-3 Functions Specifically to Modulate the ascr#8 Behavioral Response

While ascr#8 is a potent male-attracting pheromone, previous studies have shown that ascr#2, ascr#3, ascr#4 also function synergistically in attracting males [32]. The CEM neurons that are required for ascr#8 sensation also function in ascr#3 sensation [13]. While ascr#3 signal propagation is processed through the hub-and-spoke circuit centered around RMG [15,16,43], little is

known about the mechanics of ascr#8 sensation outside of CEM involvement [13]. To determine if *flp-3* functions to regulate pheromone-mediated male attraction and avoidance in a general manner, or rather one specific to ascr#8, we assayed the response of wild-type and *flp-3 lof* males to ascr#3, a cue for which behavioral valence has also recently been shown to be regulated in a sex-specific manner [15]. We found that *flp-3 lof* males exhibited no defect in their attractive response to ascr#3 (**Supp. Fig. 5**), suggesting that its role is indeed specific to that of ascr#8 sensation.

Expression analysis of a FLP-3 translational fusion (p*flp-3*::*flp-3*::mCherry) confirmed previous expression analyses of the neuropeptide within male-specific spicule neurons [33,44] (**Fig. 2J-L, Supp. Fig. 6A-C**). Transcriptional reporters have shown robust *flp-3* expression in the amphid IL1 neurons, as well as the interneurons PQR and the male-specific CP9, although our translational fusion exhibited no PQR or CP9 expression (**Fig. 2J-L, Supp. Fig. 6A-C**). Previous studies employed 1-2 kb regions of promoter sequence driving GFP expression, while our construct employs a 4 kb region, thereby incorporating further regulatory elements that may restrict expression patterns. By including the full coding sequence in our translational fusion, we have also incorporated the regulatory elements found within the introns of the *flp-3* gene [45].

Interestingly, we observed localization of mCherry within sensory cilia of the dorsal and ventral IL1 neurons, as well as in puncta spanning their dendrites (**Supp. Fig. 6D-F**), consistent with peptide packing into dense core vesicles [46]. Recent single-cell RNA-sequencing of the adult nervous system has again found more prolific expression of *flp-3* within the nervous system, including most of the VC neurons [47]. However, these studies were performed only in hermaphrodites, and were therefore unable to examine any male-specific expression changes. Our *flp-3* construct exhibits spicule- and IL1D/V-specific expression and completely rescued the

attractive response to ascr#8 (**Fig. 2G-I, Supp. Fig. 3E, F**), suggesting a physiologically relevant site-of-release from this small number of neurons.

Because the spicule neurons are exposed to the environment [48], we investigated whether they play a direct role in the sensation of ascr#8. To test this, we assayed *ceh-30 lof* males for their ability to avoid ascr#8. Male *ceh-30 lof* animals lack the male-specific CEM neurons responsible for ascr#8 sensation in the amphid region of the animal [13,49]. *him-5* males did not avoid ascr#8 (**Supp. Fig. 7**). Males lacking CEM neurons also did not avoid ascr#8 (**Supp. Fig. 7**). However, with *flp-3* still present in these animals, it may be that they are still able to sense the cue, but do not avoid it due to the presence of the neuropeptide. We therefore generated a *ceh-30;flp-3* double mutant, and found that these animals still do not avoid the pheromone (**Supp. Fig. 7**), confirming that the CEM neurons are the sole source of ascr#8 chemosensation in male *C. elegans* [13].

FLP-3 Regulates Attractive Behavior to ascr#8 by Activation of Two Evolutionarily Divergent G protein-coupled Receptors

The *flp-3* gene encodes multiple peptides [22]. Recent studies have uncovered a tenth peptide encoded by the gene; although this newest peptide does not contain the conserved GTMRFamide motif found in the remainder of *flp-3* peptides (**Fig. 3A**) [50]. We determined that the lysine-arginine sites flanking the individual peptides are processed specifically by the proprotein convertase encoded by the *egl-3* gene, and not by *aex-5* or *bli-4* [21,51,52] (**Supp. Fig. 8**), supporting previous studies that the *egl-3* gene is the proprotein convertase involved in mating behaviors [21].

To better understand where the fully processed peptides act within the male-specific circuit, we assayed mutants for receptors that have previously shown activation upon FLP-3 peptide exposure. While activation of NPR-4 has been reported for only two peptides encoded by *flp-3*,

NPR-5 and NPR-10 have been shown to respond to four and six *flp-3* encoded peptides, respectively (**Fig. 3A**) [22]. Recent studies have considered NPR-4 and NPR-10 to be representative of one another due to their close phylogenetic relationship and separation by a recent gene duplication [53]. However, in our testing of these mutants using our SWAA, we found that *npr-4* and *npr-5 lof* males respond similarly to *him-8* males (**Fig. 3B-D, Supp. Fig. 9**) while *npr-10 lof* animals exhibited a complete loss of attraction to the cue, as well as a partial avoidance phenotype matching that of *flp-3 lof* mutants (**Fig. 3B-D, Supp. Fig. 9**).

Transgenic rescue by an NPR-10::GFP translational fusion construct expressed under 1.6 kb of the endogenous promoter was able to restore wild-type levels off attraction in an *npr-10 lof* mutant background (**Fig. 3C, Supp. Fig. 9A, B**). This construct was also able to suppress the avoidance phenotype of *npr-10* (**Fig. 3D, Supp. Fig. 9C**). Expression analysis of NPR-10::GFP revealed expression in both amphid and phasmid regions of the animals (**Figure 3E, F. Supp. Fig. 9D, E**). Among these head neurons are the inner labial IL2 neurons, as well as their respective socket cells (ILso). NPR-10::GFP fluorescence was also observed in the ADL and ASG chemosensory neurons, cells which synapse onto AVD and AIA (**Fig. 7**), contributing to reversal control and turning circuitries, respectively. The localization of NPR-10 in the RMEL and RMEV neurons provides a direct input into neurons innervating muscle cells (**Fig. 3E, Fig. 7**). Alongside expression in the interneuron AVK (**Fig. 3E**), which links the *npr-10* circuitry to the backwards locomotion neuron AVE, AVF expression (**Fig. 3E**) links the circuit to the forward locomotion pre-motor interneuron, AVB (**Fig. 7**).

NPR-10 expression was also observed in the B-class ray neurons in the male tail (**Fig. 3F**). Given the tight localization of these cells, it may be that NPR-10 is also present in the HOB neuron, although without further colocalizing studies, it is impossible to tell. However, the RnB

neurons that express NPR-10 to sense SPD-secreted FLP-3 peptides heavily innervate the male-specific interneuron, EF1, which travels from the tail to synapse onto neurons in the head of the animal (**Fig. 7**), including the forward locomotion neuron, AVB. Interestingly, the hermaphrodite tail expression in the dorso-rectal ganglion neurons DVA, DVB, DVC, and ALN (**Supp. Fig. 9E**).

Using Chinese hamster ovarian (CHO) cell cultures stably expressing the promiscuous G protein, Gα16, and the calcium reporter, aequorin [54], we found that both isoforms of NPR-10 are activated by seven of the ten FLP-3 peptides (**Supp. Fig. 10A, B**), with half-maximal effective concentrations (EC_{50}) in the nM range (**Fig. 4**). Peptide FLP-3-6 (EDGNAPFGTMKFamide) did not activate NPR-10 in our assay. This peptide contains an R-to-K mutation within the C-terminal motif which may explain the lack of receptor activation. Likewise, peptide FLP-3-10 (STVDSSEPVIRDQ), which contains no sequence homology with any RFamide peptide (**Fig. 4I**) also failed to activate the receptor. Interestingly, FLP-3-8 (SADDSAPFGTMRFamide) did not activate either NPR-10A or NPR-10B, despite its conserved terminal amino acid sequence (**Supp. Fig. 10A, B**).

The lack of full avoidance phenotype observed in *npr-10 lof* mutants suggests that there are other FLP-3 receptors involved in regulating the ascr#8 avoidance behavior. Interestingly, while the short neuropeptide F receptor, NPR-10, is required for FLP-3 sensation, the *Drosophila* FR receptor homolog, FRPR-16, was also found to be reliably activated by FLP-3 peptides *in vitro* (**Supp. Fig. 10C**). This evolutionarily divergent receptor exhibited potencies in the 10-nanomolar range for seven of the peptides, and sub-micromolar for an eighth peptide (**Fig. 4**). Again, FLP-3-6 and FLP-3-10 did not activate FRPR-16, supporting the notion that the terminal motif conserved in the remaining FLP-3 peptides is critical for receptor activation. Cells

transfected with a control vector did not exhibit any activation following exposure to FLP-3 peptides, confirming that the activation observed is specific to receptor-ligand interactions with NPR-10 and FRPR-16 (**Supp. Fig. 10D**).

A full-gene deletion of *frpr-16* was generated using CRISPR mutagenesis (**Fig. 5A, B**) [55]. We assayed *frpr-16 lof* males for their ability to respond to ascr#8. Males lacking *frpr-16* exhibited a loss of attraction to ascr#8, as well as a partial avoidance phenotype, like that observed in *npr-10 lof* mutant animals (**Fig. 5, Supp. Fig. 11**). However, a double mutant containing both *npr-10* and *frpr-16* null alleles did not result in an additive effect in the avoidance phenotype, suggesting that these receptors are non-redundant in their functions (**Fig. 5E, Supp. Fig. 11C**).

Rescue of FRPR-16 under 1.9 kb of its endogenous promoter was able to restore wild-type attractive behavior (**Fig. 5C, D, Supp. Fig. 11A ,B**), as well suppress the avoidance phenotype (**Fig. 5E, Supp. Fig. 11C**). Localization of the mCherry fusion reporter was observed in the pre-motor interneurons responsible for reverse locomotory control: AVA, AVE, and AVD (**Fig. 5F**). The fluorescent protein was also seen anterior to the nerve ring in the gas-sensing BAG neuron (**Fig. 5F**). This expressing pattern was not sex-specific, as a matching expression pattern was observed in hermaphrodites (**Supp. Fig. 11D**). Together, these data show that NPR-10 and FRPR-16 function as receptors for FLP-3 peptides.

Rescue of Individual FLP-3 Peptides by Feeding Reveals a Specific Subset of Active Peptides Required for Attractive Behavior

To identify which FLP-3 peptides are required for male avoidance of ascr#8, we adopted a peptide feeding approach, similar to RNAi feeding, as initially described previously [36]. Using Gateway Cloning technology, we first inserted the peptide coding sequences for the FLP-3

peptides unable to rescue the ascr#8 response in the *ok3625* allele (**Supp. Fig. 4**), FLP-3-1 (SPLGTMRFamide) and FLP-3-4 (NPLGTMRFamide) in our assays (**Fig. 6**). *flp-3 lof* animals were grown on lawns of bacteria expressing the rescue constructs, and their progeny were tested by both SWAA and avoidance assays (**Fig. 6B-D, Supp. Fig. 12**). Peptides FLP-3-1 and FLP-3-4 were unable to rescue either phenotype on their own (**Fig. 6B-D, Supp. Fig. 12**), supporting the *flp-3(ok3625)* data suggesting that these two peptides are insufficient to maintain wild-type behavior (**Supp Fig. 4**).

FLP-3-1 and FLP-3-4 differ in sequence only in their N-terminal amino acid. Similarly, a single amino acid change is all that distinguishes them from FLP-3-2 (TPLGTMRFamide), which we then tested for its ability to rescue the *flp-3 lof* phenotype. Surprisingly, this peptide was able to abolish the avoidance phenotype observed in *flp-3 lof* animals (**Fig. 6B, Supp. Fig. 12A**). However, it was not able to restore the animal's ability to be attracted to ascr#8 (**Fig. 6 C,D, Supp. Fig. 12C**). The only difference being the presence of a threonine in that position of the peptide, we hypothesized that this may be the required component to suppress the avoidance behavior. Peptide FLP-3-9 (NPENDTPFGTMRFamide) contains a threonine in the same location of the peptide. The N-terminus is capped with a NPEND sequence, and the lysine conserved in FLP-3-1, 3-2, and 3-4 is mutated to a phenylalanine. However, when *flp-3 lof* animals were fed NPENDTPFGTMRFamide, they not only displayed lack of avoidance to ascr#8, but a full rescue of their ability to be attracted to the cue (**Fig. 6, Supp. Fig. 12**). We also tested FLP-3-10 (STVDSSEPVIRDQ), which exhibits a lack of consensus sequence and an inability to activate either NPR-10 or FRPR-16. The non-RFamide peptide was unsurprisingly unable to rescue the avoidance phenotype (**Fig. 6B, Supp. Fig. 12A**).

We hypothesize that the threonine in the ninth position from the C-terminus is critical for suppression of the basal avoidance response, as both FLP-3-2 and FLP-3-9 were capable of doing so, while FLP-3-1 and FLP-3-4 were not (**Fig. 6, Supp. Fig. 12**). Likewise, the NPEND sequence in FLP-3-9 may convey specificity to the peptide, allowing it to drive attraction to the pheromone.

Discussion

Our results reveal a complex mechanism regulating the sex-specific behavioral response to a pheromone guided through the interaction of two peptides encoded by a single neuropeptide precursor gene and two divergent GPCRs. Peptidergic modulation of neural circuits has long been hypothesized as complex [56], and here we elucidate the recruitment of two neuropeptide/neuropeptide-receptor (NP/NPR) modules, FLP-3/NPR-10 and FLP-3/FRPR-16, that both serve to regulate the nervous system in sensing and respond to asr#8 in a sex-specific manner. Our results elucidate that not all of the peptides encoded by the FLP-3 pro-peptide are involved in the regulation of the sex-specific circuit, but rather a subset function through two unique NP/NPR modules to drive the behavioral response. The involvement of two evolutionarily divergent receptors in sensing specific FLP-3 neuropeptides suggests that the sex-specific behavioral response to ascr#8 module is a result of the activity of two distinct NP/NPR modules that mediate both attractive and repulsive properties of the small molecule.

These findings are consistent with neuromodulators regulating behavioral states in both invertebrates and vertebrates. Multiple hormonal receptors are involved in regulating the induction of *A. aegyptii* ecdysteroid hormone production through two different neuropeptide signaling systems: ILP3 initiates digestion of the blood meal [57], while OEH stimulates oocyte yolk uptake [58]. Melanin-concentrating hormone is a neuropeptidergic hormone that promotes

appetite and feeding behaviors in mice in a sex-dependent manner [59]. Meanwhile, age-dependent changes in levels of Neuropeptide F result in the promotion of survival-benefiting appetitive memory in *Drosophila*, concurrent with the impairment of memories associated with insufficient survival benefits [60].

Here, we show that two NP/NPR modules driven by the single neuropeptide gene *flp-3* serve to drive sex-specific attraction to the male attracting pheromone, ascr#8 [13,27] (**Fig. 2**). These modules serve to simplify the immensely complex peptidergic connectome of the nervous system [56]. Hermaphrodites avoid the pheromone, regardless of the presence of *flp-3* (**Fig. 2F**), while males lacking any component of the two NP/NPR modules "revert" to the hermaphroditic response (**Fig. 2C**).

This suggests that the complexity of the expansive class of FMRFamide-related peptide (FLP) genes in *C. elegans*, of which there are 31 genes encoding over 70 unique peptides [41], function through an even greater number of NP/NPR modules to drive specific behavioral or physiological states. FLPs have been identified as regulators of a variety of behavioral and sensory mechanisms, including locomotion [18], egg-laying [41], gas sensing [61], sleep [28], and mating [21,62]. Here, we show that *flp-3* functions to coordinate ascr#8 sensation with attractive behavior. Not every male is attracted to ascr#8, as only 30-45% of males exhibit attractive responses (**Supp. Fig. 2B**), which interestingly matches well with the rate of CEM chemosensory neuron calcium transient activity upon exposure to mating ascarosides [38].

Two GPCRs respond to FLP-3 peptides to function in the behavioral response to ascr#8: the previously identified NPR-10, and the novel FRPR-16 (**Fig. 3-5**). Both exhibit high potencies for multiple FLP-3 peptides, although our single peptide rescues have shown that FLP-3-2 and FLP-3-9 are required for the wild-type response to ascr#8 (**Fig. 6**), while FLP-3-1, FLP-3-4, and FLP-

3-10 are not. As such, multiple NP/NPR modules are implicated in the ascr#8 behavioral response. Further studies will allow for further separation of FLP-3-2 and FLP-3-9, and how they interact with NPR-10 and FRPR-16.

Interestingly, these two high-potency FLP-3 receptors are divergent in their evolutionary history. NPR-10 is most related to other "NPR" *C. elegans* receptors that evolved from the same family as the *Drosophila melanogaster* short neuropeptide F receptor family [63,64]. FRPR-16, however, is more closely related to the fly FMRFamide Receptor [65]. Interestingly, while some *C. elegans* FRPRs function as FLP receptors [18,62,66], at least one receptor within the same evolutionary clade (DAF-37) acts as a chemosensor for pheromones [67].

The presence of FRPR-16 in the amphid pre-motor interneurons responsible for backwards locomotion (**Fig. 5**) suggests the FLP-3/FRPR-16 module serves to mediate reversals during ascr#8 sensation (**Fig. 7**). Conversely, while FRPR-16 is confined to a small, yet biologically specific subset of neurons in the head of the animals, NPR-10 exhibits more promiscuous expression that innervates both forward and reverse locomotion circuitries (**Fig 3E, F**). As such, while the FLP-3/FRPR-16 module specifically modulates reversals, the FLP-3/NPR-10 module may instead serve to balance both forward and backwards locomotion in response to ascr#8, allowing the animal to more thoroughly interrogate its surroundings. Future studies incorporating cell-specific rescue of both NPR-10 and FRPR-16 will further elucidate this circuitry.

We pose that the EF1 circuitry connecting the tail to the amphid pre-motor neurons, inferred from the physical male connectome [68] (**Fig. 7**), serves to suppress forward locomotion: as the male travels down an ascr#8 concentration gradient, information travels from the tail to the head, driving the animal to return to the ascr#8-containing region. How this sensation occurs, given

that the amphid CEM neurons are the sole source of ascr#8 sensation (**Supp. Fig. 7**), remains a mystery.

Previous studies have linked the entirety of the gene to a receptor based on binding studies and full transgenic rescue [28,66,69]. Here, we employ a rescue-by-feeding assay, following the design of RNAi feeding protocols, to rescue individual peptides [36]. While "feeding" of peptides through soaking is a valid approach, there are many constraints on such approaches, the most prominent being the ability to acquire purified peptides [28,66]. Using our rescue-by-feeding approach, we provide access to the peptide to the worms directly through their food source. Combining biochemical receptor activation studies with behavioral rescue-by-feeding assays, we have been successful in elucidating discrete neuropeptide signaling modalities within the complex FLP-3 signaling system. This approach enables new avenues for characterizing the roles of the other neuropeptides in mediating diverse cellular and organismal processes.

In summary, we demonstrate that specific peptides encoded by *flp-3*, expressed in neurons of both the male head and tail, activate evolutionarily divergent receptors. These two NP/NPR modules mediate overlapping behavioral outputs, resulting the fine-tuned sex-specific behavioral response to ascr#8 by simultaneously suppressing an avoidance response and driving an attractive response (**Fig. 7**). The entirety of the *flp-3* gene is not required to recapitulate wild-type behavior, suggesting that individual peptides from a single gene are involved in discrete NP/NPR modules.

Methods

Strains

Strains were obtained from the *Caenorhabditis* Genetics Center (University of Minnesota, MN), the National BioResource Project (Tokyo Women's Medical University, Tokyo, Jagan), Chris Li at City University of New York, Paul Sternberg at the California Institute of Technology, Ding Xue at University of Colorado Boulder, and Maureen Barr at Rutgers University. The novel allele of *frpr-16* was generated via CRISPR editing using previously discussed methods [55]. Strains were crossed with either *him-5* or *him-8* worms to generate stable males prior to testing. See **Supp. Table. 1** for a comprehensive list of strains used in this study.

Vector Generation

Peptide constructs: DNA oligos containing the sequence for the peptides of interest were generated using Integrated DNA Technologies' Ultramer synthesis service. The DNA sequence encoding the peptide sequence was flanked with sequences encoding EGL-3 cut sites (MRFGKR upstream, and KRK-STOP) downstream. These sites were then flanked with Gateway Cloning sites attB1 and attB2. Annealed oligos were then used to perform a BP reaction with pDONR p1-p2 to generate the pENTRY clones. These vectors where then recombined with pDEST-527 (a gift from Dominic Esposito (Addgene plasmid # 11518) in LR reactions to generate the expression clones. The SCRAMBLE control was generated in an identical manner, with the sequence between the cut sites being amplified from pL4440 (provided by Victor Ambros, University of Massachusetts Medical School, MA).

Fusion constructs: DNA for the *flp-3, npr-10,* and *frpr-16* promoter and coding regions were isolated from *C. elegans* genomic DNA via PCR.

In generating the *flp-3* rescue product, PstI and BamHI restriction sites added onto the isolated fragments were introduced through primer design. PCR amplicons and the Fire GFP Vector, pPD95.75 (kindly provided by Josh Hawk, Yale University, CT), were digested with PstI and BamHI enzymes. Products were ligated together to generate JSR#DKR18 (p*flp-3*::*flp-3*::GFP). The *flp-3* expression analysis construct, JSR#DKR34 (p*flp-3*::*flp-3*::SL2::mCherry) was generated by Genewiz. The promoter-gene fragment of *npr-10* was generated by Gibson Assembly to GFP (from pPD95.75) and as a linear fusion. The rescue-fusion construct of *frpr-16* was achieved by fusing the promoter and gene sequence to mCherry isolated from JSR#DKR34 via Gibson Assembly.

See **Supp. Table 2** for a complete plasmid list, and **Supp. Table 3** for primer and Ultramer sequences.

Transgenic Animals

CB1489 animals were injected with JSR#DKR18 (p*flp-3*::*flp-3*::GFP at 20 ng/µL), using p*unc-122*::RFP (at 20 ng/µL) (kindly provided by Sreekanth Chalasani at the Salk Institute, CA) as a co-injection marker to generate JSR81 (*him-8*(e1489);worEx17[p*flp-3*::*flp-3*::GFP; p*unc-122*::RFP]). JSR81 was then crossed with JSR99 to generate JSR109 (*flp-3*(*pk361*);*him-8*(e1489);worEx17[p*flp-3*::*flp-3*::GFP; p*unc-122*::RFP]).

PS2218 animals were injected with JSR#DKR34 (p*flp-3*::*flp-3*::SL2::mCherry at 25 ng/µL), using p*unc-122*::GFP (at 50 ng/µL) as a co-injection marker to generate JSR119 (*dpy-20*(e1362);*him-5*(e1490);syls33[HS.C3(50ng/µL) + pMH86(11ng/µL)];worEx21[*pflp-3*::*flp-3*::SL2::mCherry; *punc-122*::GFP]).

JSR102 animals were injected with a linear fusion product (p*npr-10*::*npr-10*::GFP at 25 ng/µL), alongside p*unc-122*::RFP (at 50 ng/µL) as a co-injection marker to generate JSR126

(*npr-10*(*tm8982*);*him-8*(e1489);worEx37[p*npr-10*::*npr-10*::GFP, p*unc-122*::RFP]). This was crossed with PT2727 (myIS20 [p*klp-6*::tdTomato + pBX], a gift from Maureen Barr) to generate JSR138 (myIS20 [p*klp-6*::tdTomato, pBX]; *npr-10*(*tm8982*);*him-8*(e1489);worEx37[p*npr-10*::*npr-10*::GFP, p*unc-122*::RFP]).

JSR103 animals were injected with a linear fusion product (p*frpr-16*::*frpr-16*::SL2::mCherry at 25 ng/µL), alongside p*unc-122*::GFP (at 50 ng/µL) as a co-injection marker to generate JSR133 (*frpr-16*(gk5305[loxP + p*myo-2*::GFP::*unc-54* 3' UTR + p*rps-27*::neoR::*unc-54* 3' UTR + loxP]);*him-8*(e1489);worEx41[p*frpr-16*::*frpr-16*::SL2::mCherry, p*unc-122*::GFP]).

Injections for JSR81 were generously performed by the Alkema Lab at UMass Medical School. Injections for JSR119, JSR126, and JSR133 were performed by In Vivo Biosystems (formerly NemaMetrix).

Chemical Compounds

The ascarosides ascr#3 and ascr#8 were synthesized as described previously [27,32]. Peptides used in *in vitro* GPCR activation assays were synthesized by GL Biochem Ltd.

Spot Retention Assay

Assays were performed as described previously [13,32]. 50-60 larval-stage 4 (L4) males were segregated by sex and stored at 20 °C for 5 hours to overnight to be assayed as young adults. For hermaphrodite trials, young adult hermaphrodites were segregated 1.5 hours prior to testing. 0.6 µL of vehicle control or ascaroside #8 was placed in each scoring region (**Supp. Fig. 1A**). As the working stock of ascaroside #8 was made in MilliQ-purified ultrapure H_2O, this was used as the vehicle control. Five animals were placed on each "X" the assay plate (**Supp. Fig. 1A**), which was then transferred to a microscope containing a camera and recorded for 20 minutes. Each strain and sex were assayed over five plates per day on at least three different days.

494 **Single Worm Assay**

495 The outer forty wells of a 48-well suspension culture plate (Olympus Plastics, Cat #: 25-103)
496 were seeded with 200 µL of standard NGM agar. To prepare the plates for the assay, they were
497 acclimated to room temperature, at which point each well was seeded with 65 µL of OP50 *E.*
498 *coli*. The assay plates were then transferred to a 37 °C incubator with the lid tilted for 4 hours to
499 allow the bacterial culture to dry on the agar. Once the bacterial culture dried, the lid was
500 replaced the plate was stored at 20 °C until used in the assay. 50-60 L4 worms were segregated
501 by sex and stored at 20 °C for 5 hours to overnight to be assayed as young adults. 0.8 µL of
502 either vehicle control or ascaroside #8 was placed in the center of the well corresponding to that
503 condition within the quadrant being tested, following a random block design (**Fig. 1A**). A single
504 worm was placed in each of the 10 wells to be assayed, and the plate was transferred to a light
505 source and camera and recorded for 15 minutes. This process was repeated for all four quadrants.
506 Each strain and sex were assayed over five plates assayed on at least three different days.

507 **Raw Dwell Time**

508 Raw dwell time values were calculated by subtracting the time a worm exited the cue (center of
509 the well in spatial controls), from the time it entered, as in the SRA [13]. This was determined per
510 visit, and the average dwell time was calculated for each animal in the quadrant. Averages of the
511 four-quadrant means were determined per plate, and a minimum of five plates were assayed per
512 strain/condition. The mean raw dwell time across five plates was calculated and used for
513 statistical analyses and graphical display.

514 **Log(fold-change)**

515 The average dwell time in the ascaroside was divided by the average dwell time within the
516 vehicle control per plate to generate a fold-change. To transform the data, the log of this fold-

change was taken, and the average log(fold-change) was used for statistical analyses and graphical display.

Visit Count

The number of visits per worm was calculated, and the average visit count determined per quadrant, and per plate. The average visit count across five plates was calculated and used for statistical analyses and graphical display.

Percent Attractive Visits

An "attractive visit" was first determined for each plate as any visit greater than two standard deviations above the mean dwell time within the vehicle control for that plate. Any individual visit meeting this threshold was scored as a "1", and any below was scored a "0". The percent visits per worm that were attractive was determined, and the average of each quadrant taken. The four quadrant values were then averaged to generate plate averages. The average percent of attractive visits across five plates was calculated and used for statistical analyses and graphical display.

Avoidance Assay

Assays were performed as described previously [4,10,40]. 50-60 L4 worms were segregated by sex and stored at 20 °C for 5 hours to overnight to be assayed as young adults. 1-4 hours prior to the assay, the lids of unseeded plates were tilted to allow any excess moisture to evaporate off the plates. At the time of the assay, 10 or more animals were transferred onto each of the dried, unseeded plates. A drop of either water or 1 µM ascr#8 was placed on the tail of forward moving animals, and their response was scored as either an avoidance response, or no response. The total number of avoidances was divided by the total number of drops to generate an avoidance index for that plate. This was repeated for at least 10 plates over at least three different days.

Statistical Analyses

Spot Retention Assay

Statistical comparisons within each strain were made by Paired t-tests. For comparisons between strains/conditions, the data was transformed as described previously [37]. In short, the data was transformed to have only non-zero data for the calculation of fold-changes. This was done using a Base 2 Exponentiation (2^n, where n is equal to the dwell time). The log (base 2) of the fold-changes of these transformed values was used to allow for direct comparisons between strains of the same background (i.e., *him-5* and *osm-3;him-5*) using a Student's t-test. *p*-values are defined in respective figure captions, with thresholds set as: * $p < 0.05$, ** $p < 0.01$, *** $p < 0.001$, **** $p < 0.0001$.

Single Worm Assay

Statistical comparisons within each strain/sex (spatial, vehicle, ascaroside) were made by Repeated Measured ANOVA with the significance level set at 0.05, followed by multiple comparisons using Bonferroni correction. For comparisons between strains/sexes, the spatial control dwell times were compared using a one-way ANOVA followed by a Dunnett's correction to confirm that mutations of interest had no effect on the amount of time animals naturally spent in the center of the well. To directly compare strains, a fold-change was calculated by dividing the ascaroside by vehicle dwell times for each assay. This was then transformed by taking the log (base 10) of the fold-change. Comparisons were then made by One-Way ANOVA followed by multiple comparisons using Dunnett's correction. *p*-values are defined in respective figure captions, with thresholds set as: * $p < 0.05$, ** $p < 0.01$, *** $p < 0.001$, **** $p < 0.0001$.

562 **Avoidance Assay**

563 Statistical comparisons within each strain were made by paired t-test against a significance level
564 set at 0.05. For comparisons between strains/conditions, comparisons were made by One-Way
565 ANOVA, followed by multiple comparisons using Bonferroni correction. *p*-values are defined in
566 respective figure captions, with thresholds set as: * $p < 0.05$, ** $p < 0.01$, *** $p < 0.001$, **** p
567 < 0.0001.

568 ***In vitro* GPCR activation assay**

569 The GPCR activation assay was performed as previously described [69,70]. Briefly, *npr-10* and
570 *frpr-16* cDNAs were cloned into the pcDNA3.1 TOPO expression vector (Thermo Fisher
571 Scientific). A CHO-K1 cell line (PerkinElmer, ES-000-A24) stably expressing apo-aequorin
572 targeted to the mitochondria (mtAEQ) and human Gα16 was transiently transfected with the
573 receptor cDNA construct or the empty pcDNA3.1 vector using Lipofectamine LTX and Plus
574 reagent (Thermo Fisher Scientific). Cells were shifted to 28°C one day later and allowed to
575 incubate for 24 h. On the day of the assay, cells were collected in BSA medium (DMEM/Ham's
576 F12 with 15 mM HEPES, without phenol red, 0.1% BSA) and loaded with 5 mM coelenterazine
577 h (Thermo Fisher Scientific) for 4 h at room temperature. The incubated cells were then added to
578 synthetic peptides dissolved in DMEM/BSA, and luminescence was measured for 30 s at 496 nm
579 using a Mithras LB940 (Berthold Technologies) or MicroBeta LumiJet luminometer
580 (PerkinElmer). After 30 s of readout, 0.1 % triton X-100 was added to lyse the cells, resulting in
581 a maximal calcium response that was measured for 10 s. After initial screening, concentration-
582 response curves were constructed for HPLC-purified FLP-3 peptides by subjecting the
583 transfected cells to each peptide in a concentration range from 1 pM to 10 μM. Cells transfected
584 with an empty vector were used as a negative control. Assays were performed in triplicate on at

least two independent days. Concentration-response curves were fitted using Prism v. 7 (nonlinear regression analysis with a sigmoidal concentration-response equation).

Generation of a Null *frpr-16* Mutant by CRISPR Mutagenesis

The *frpr-16* CRISPR/Cas9 knockout was provided by the Vancouver node of the International *C. elegans* Consortium. The mutation was generated following previously described techniques [55]. In short, a 1685 bp region containing the coding sequence, as well 52 bp upstream and 60 bp downstream, was removed from the genome, and replaced with a trackable cassette containing p*myo-2*::GFP and a neomycin resistance gene (**Fig 5A, B**). The flanking sequences of the mutated sequence are TCATAATTGTTTGTTTGACAAAAACCGGGA and GGTGGAAACGGAAATGAAAGAAAAAACCGA. PCR confirmation of gene replacement with cassette was performed via four sets of PCR reactions checking the upstream insertion site and the downstream insertion site in the mutant strain, and a test for wild-type sequence in both mutant and wild-type strains. A band is present on the gel in wild-type samples, with no band present in the mutant, as a primer sequence is removed with the cassette insertion.

See **Supp. Table 3** for primer sequences.

Peptide Rescue

SCRAMBLE control or FLP-3 peptide constructs were grown overnight in LB media containing 50 µg/µL ampicillin at 37 °C and diluted to an OD_{600} of 1.0 prior to seeding on NGM plates containing 50 µg/µL ampicillin and 1 mM IPTG. The 75 µL lawn was left to dry and grow overnight at room temperature before 3 L4 animals were placed on the plates. Males were selected for testing in the same manner as described above but were isolated onto plates also seeded with the same peptide on which they had been reared. Animals were then assayed using either the Avoidance Assay or Single Worm Assay.

608 **Imaging**

609 Animals were mounted on a 2% agar pad and paralyzed using 1 M sodium azide on a
610 microscope slide, as described previously [10].

611 Images for amphid *flp-3* expression were acquired using a Zeiss LSM700 confocal
612 microscope. Final images were obtained using a 63x oil objective with a 1.4x digital zoom, for a
613 final magnification of ~90X. Tail images were acquired using a Zeiss Apotome using a 40x oil
614 objective.

615 Images of *npr-10* and *frpr-16* expression were acquired using a Zeiss LSM510 Meta inverted
616 confocal microscope. Final images of *npr-10* were obtained using a 63x oil objective with a 0.8x
617 digital zoom, for a final magnification of ~50X. Final images of *frpr-16* were obtained at either
618 20x (air objective) or 63x (oil) with a 2x digital zoom, for a final magnification of ~125x.

619

620

621 **References**

622 1 García, L. R. & Portman, D. S. Neural circuits for sexually dimorphic and sexually
623 divergent behaviors in *Caenorhabditis elegans*. *Curr Opin Neurobiol* **38**, 46-52,
624 doi:10.1016/j.conb.2016.02.002 (2016).
625 2 Li, Y. & Dulac, C. Neural coding of sex-specific social information in the mouse brain.
626 *Current Opinion in Neurobiology* **53**, 120-130, doi:10.1016/j.conb.2018.07.005 (2018).
627 3 Yang, T. & Shah, N. M. Molecular and neural control of sexually dimorphic social
628 behaviors. *Current opinion in neurobiology* **38**, 89-95, doi:10.1016/j.conb.2016.04.015
629 (2016).
630 4 Chute, C. D. & Srinivasan, J. Chemical mating cues in *C. elegans*. *Semin Cell Dev Biol*
631 **33**, 18-24, doi:10.1016/j.semcdb.2014.06.002 (2014).
632 5 Kaba, H., Fujita, H., Agatsuma, T. & Matsunami, H. Maternally inherited peptides as
633 strain-specific chemosignals. *Proc Natl Acad Sci U S A*, doi:10.1073/pnas.2014712117
634 (2020).
635 6 McGrath, P. T. & Ruvinsky, I. A primer on pheromone signaling in *Caenorhabditis*
636 *elegans* for systems biologists. *Current opinion in systems biology* **13**, 23-30,
637 doi:10.1016/j.coisb.2018.08.012 (2019).
638 7 Silva, L. & Antunes, A. Vomeronasal Receptors in Vertebrates and the Evolution of
639 Pheromone Detection. *Annual review of animal biosciences* **5**, 353-370,
640 doi:10.1146/annurev-animal-022516-022801 (2017).
641 8 Flavell, S. W., Raizen, D. M. & You, Y.-J. Behavioral States. *Genetics* **216**, 315-332,
642 doi:10.1534/genetics.120.303539 (2020).

643 9 Ghosh, D. D. *et al.* Neural Architecture of Hunger-Dependent Multisensory Decision
644 Making in C. elegans. *Neuron* **92**, 1049-1062, doi:10.1016/j.neuron.2016.10.030 (2016).
645 10 Chute, C. D. *et al.* Co-option of neurotransmitter signaling for inter-organismal
646 communication in *C. elegans*. *Nat Commun* **10**, 3186, doi:10.1038/s41467-019-11240-7
647 (2019).
648 11 Barr, M. M., García, L. R. & Portman, D. S. Sexual Dimorphism and Sex Differences in
649 *Caenorhabditis elegans* Neuronal Development and Behavior. *Genetics* **208**, 909-935,
650 doi:10.1534/genetics.117.300294 (2018).
651 12 Virk, B. *et al.* Folate Acts in *E. coli* to Accelerate *C. elegans* Aging Independently of
652 Bacterial Biosynthesis. *Cell Rep* **14**, 1611-1620, doi:10.1016/j.celrep.2016.01.051 (2016).
653 13 Narayan, A. *et al.* Contrasting responses within a single neuron class enable sex-specific
654 attraction in *Caenorhabditis elegans*. *Proc Natl Acad Sci U S A* **113**, E1392-1401,
655 doi:10.1073/pnas.1600786113 (2016).
656 14 Aprison, E. Z. & Ruvinsky, I. Counteracting Ascarosides Act through Distinct Neurons
657 to Determine the Sexual Identity of *C. elegans* Pheromones. *Curr Biol* **27**, 2589-
658 2599.e2583, doi:10.1016/j.cub.2017.07.034 (2017).
659 15 Fagan, K. A. *et al.* A Single-Neuron Chemosensory Switch Determines the Valence of a
660 Sexually Dimorphic Sensory Behavior. *Curr Biol* **28**, 902-914.e905,
661 doi:10.1016/j.cub.2018.02.029 (2018).
662 16 Jang, H. *et al.* Neuromodulatory state and sex specify alternative behaviors through
663 antagonistic synaptic pathways in *C. elegans*. *Neuron* **75**, 585-592,
664 doi:10.1016/j.neuron.2012.06.034 (2012).

17 Barrios, A., Ghosh, R., Fang, C., Emmons, S. W. & Barr, M. M. PDF-1 neuropeptide signaling modulates a neural circuit for mate-searching behavior in *C. elegans*. *Nature Neuroscience* **15**, 1675-1684, doi:10.1038/nn.3253 (2012).

18 Chen, D., Taylor, K. P., Hall, Q. & Kaplan, J. M. The Neuropeptides FLP-2 and PDF-1 Act in Concert To Arouse *Caenorhabditis elegans* Locomotion. *Genetics* **204**, 1151-1159, doi:10.1534/genetics.116.192898 (2016).

19 Hilbert, Z. A. & Kim, D. H. PDF-1 neuropeptide signaling regulates sexually dimorphic gene expression in shared sensory neurons of *C. elegans*. *eLife* **7**, e36547, doi:10.7554/eLife.36547 (2018).

20 Ryu, L. *et al.* Feeding state regulates pheromone-mediated avoidance behavior via the insulin signaling pathway in *Caenorhabditis elegans*. *The EMBO journal* **37**, e98402, doi:10.15252/embj.201798402 (2018).

21 Liu, T., Kim, K., Li, C. & Barr, M. M. FMRFamide-like neuropeptides and mechanosensory touch receptor neurons regulate male sexual turning behavior in *Caenorhabditis elegans*. *J Neurosci* **27**, 7174-7182, doi:10.1523/JNEUROSCI.1405-07.2007 (2007).

22 Li, C. & Kim, K. Family of FLP Peptides in *Caenorhabditis elegans* and Related Nematodes. *Front Endocrinol (Lausanne)* **5**, 150, doi:10.3389/fendo.2014.00150 (2014).

23 Hung, W. L. *et al.* Attenuation of insulin signalling contributes to FSN-1-mediated regulation of synapse development. *The EMBO Journal* **32**, 1745-1760, doi:10.1038/emboj.2013.91 (2013).

686 24 Leinwand, S. G. & Chalasani, S. H. Neuropeptide signaling remodels chemosensory
687 circuit composition in *Caenorhabditis elegans*. *Nature neuroscience* **16**, 1461-1467,
688 doi:10.1038/nn.3511 (2013).
689 25 Bhardwaj, A., Thapliyal, S., Dahiya, Y. & Babu, K. FLP-18 Functions through the G-
690 Protein-Coupled Receptors NPR-1 and NPR-4 to Modulate Reversal Length in
691 *Caenorhabditis elegans*. *The Journal of Neuroscience* **38**, 4641,
692 doi:10.1523/JNEUROSCI.1955-17.2018 (2018).
693 26 Yu, Y., Zhi, L., Guan, X., Wang, D. & Wang, D. FLP-4 neuropeptide and its receptor in a
694 neuronal circuit regulate preference choice through functions of ASH-2 trithorax complex
695 in *Caenorhabditis elegans*. *Sci Rep* **6**, 21485, doi:10.1038/srep21485 (2016).
696 27 Pungaliya, C. *et al.* A shortcut to identifying small molecule signals that regulate
697 behavior and development in *Caenorhabditis elegans*. *Proceedings of the National*
698 *Academy of Sciences of the United States of America* **106**, 7708-7713,
699 doi:10.1073/pnas.0811918106 (2009).
700 28 Iannacone, M. J. *et al.* The RFamide receptor DMSR-1 regulates stress-induced sleep in
701 *C. elegans*. *Elife* **6**, doi:10.7554/eLife.19837 (2017).
702 29 Beets, I. *et al.* Natural Variation in a Dendritic Scaffold Protein Remodels Experience-
703 Dependent Plasticity by Altering Neuropeptide Expression. *Neuron*, S0896-
704 6273(0819)30849-30849, doi:10.1016/j.neuron.2019.10.001 (2019).
705 30 Hussey, R. *et al.* Oxygen-sensing neurons reciprocally regulate peripheral lipid
706 metabolism via neuropeptide signaling in *Caenorhabditis elegans*. *PLoS genetics* **14**,
707 e1007305-e1007305, doi:10.1371/journal.pgen.1007305 (2018).

31 Ringstad, N. & Horvitz, H. R. FMRFamide neuropeptides and acetylcholine synergistically inhibit egg-laying by *C. elegans*. *Nat Neurosci* **11**, 1168-1176, doi:10.1038/nn.2186 (2008).

32 Srinivasan, J. *et al.* A blend of small molecules regulates both mating and development in *Caenorhabditis elegans*. *Nature* **454**, 1115-1118, doi:10.1038/nature07168 (2008).

33 Kim, K. & Li, C. Expression and regulation of an FMRFamide-related neuropeptide gene family in *Caenorhabditis elegans*. *J Comp Neurol* **475**, 540-550, doi:10.1002/cne.20189 (2004).

34 Fenk, L. A. & de Bono, M. Memory of recent oxygen experience switches pheromone valence in *Caenorhabditis elegans*. *Proceedings of the National Academy of Sciences* **114**, 4195, doi:10.1073/pnas.1618934114 (2017).

35 Rengarajan, S., Yankura, K. A., Guillermin, M. L., Fung, W. & Hallem, E. A. Feeding state sculpts a circuit for sensory valence in *Caenorhabditis elegans*. *Proceedings of the National Academy of Sciences* **116**, 1776, doi:10.1073/pnas.1807454116 (2019).

36 Xu, J. *et al.* Feeding recombinant *E. coli* with GST-mBmKTX fusion protein increases the fecundity and lifespan of *Caenorhabditis elegans*. *Peptides* **89**, 1-8, doi:10.1016/j.peptides.2017.01.003 (2017).

37 Zhang, Y. K., Reilly, D. K., Yu, J., Srinivasan, J. & Schroeder, F. C. Photoaffinity probes for nematode pheromone receptor identification. *Journal of Organic & Biomolecular Chemistry*, 10.1039/c1039ob02099c, doi:10.1039/c9ob02099c (2019).

38 Reilly, D. K., Lawler, D. E., Albrecht, D. R. & Srinivasan, J. Using an Adapted Microfluidic Olfactory Chip for the Imaging of Neuronal Activity in Response to

730 Pheromones in Male *C. Elegans* Head Neurons. *Journal of Visualized Experiments*,
731 e56026, doi:doi:10.3791/56026 (2017).
732 39 Greene, J. S. *et al.* Balancing selection shapes density-dependent foraging behaviour.
733 *Nature* **539**, 254-258, doi:10.1038/nature19848 (2016b).
734 40 Hilliard, M. A., Bergamasco, C., Arbucci, S., Plasterk, R. H. A. & Bazzicalupo, P.
735 Worms taste bitter: ASH neurons, QUI-1, GPA-3 and ODR-3 mediate quinine avoidance
736 in *Caenorhabditis elegans*. *The EMBO Journal* **23**, 1101-1111,
737 doi:10.1038/sj.emboj.7600107 (2004).
738 41 Chang, Y.-J. *et al.* Modulation of Locomotion and Reproduction by FLP Neuropeptides
739 in the Nematode *Caenorhabditis elegans*. *PLoS ONE* **10**, e0135164,
740 doi:10.1371/journal.pone.0135164 (2015).
741 42 Yemini, E., Jucikas, T., Grundy, L. J., Brown, A. E. X. & Schafer, W. R. A database of
742 *Caenorhabditis elegans* behavioral phenotypes. *Nature Methods* **10**, 877-879,
743 doi:10.1038/nmeth.2560 (2013).
744 43 Macosko, E. Z. *et al.* A Hub-and-Spoke Circuit Drives Pheromone Attraction and Social
745 Behavior in *C. elegans*. *Nature* **458**, 1171-1175, doi:10.1038/nature07886 (2009).
746 44 Jiang, L. I. & Sternberg, P. W. An HMG1-like protein facilitates Wnt signaling in
747 *Caenorhabditis elegans*. *Genes Dev* **13**, 877-889 (1999).
748 45 Puckett Robinson, C., Schwarz, E. M. & Sternberg, P. W. Identification of DVA
749 interneuron regulatory sequences in *Caenorhabditis elegans*. *PLoS One* **8**, e54971,
750 doi:10.1371/journal.pone.0054971 (2013).

751 46 Laurent, P. *et al.* Genetic dissection of neuropeptide cell biology at high and low activity
752 in a defined sensory neuron. *Proceedings of the National Academy of Sciences* **115**,
753 E6890, doi:10.1073/pnas.1714610115 (2018).
754 47 Taylor, S. R. *et al.* Expression profiling of the mature *C. elegans* nervous system by
755 single-cell RNA-Sequencing. *bioRxiv*, 737577, doi:10.1101/737577 (2019).
756 48 Sulston, J. E., Albertson, D. G. & Thomson, J. N. The *Caenorhabditis elegans* male:
757 postembryonic development of nongonadal structures. *Dev Biol* **78**, doi:10.1016/0012-
758 1606(80)90352-8 (1980).
759 49 Peden, E., Kimberly, E., Gengyo-Ando, K., Mitani, S. & Xue, D. Control of sex-specific
760 apoptosis in *C. elegans* by the BarH homeodomain protein CEH-30 and the
761 transcriptional repressor UNC-37/Groucho. *Genes Dev* **21**, 3195-3207,
762 doi:10.1101/gad.1607807 (2007).
763 50 Van Bael, S. *et al.* A *Caenorhabditis elegans* Mass Spectrometric Resource for
764 Neuropeptidomics. *Journal of The American Society for Mass Spectrometry*,
765 doi:10.1007/s13361-017-1856-z (2018).
766 51 Husson, S. J., Clynen, E., Baggerman, G., Janssen, T. & Schoofs, L. Defective processing
767 of neuropeptide precursors in *Caenorhabditis elegans* lacking proprotein convertase 2
768 (KPC-2/EGL-3): mutant analysis by mass spectrometry. *J Neurochem* **98**, 1999-2012,
769 doi:10.1111/j.1471-4159.2006.04014.x (2006).
770 52 Thacker, C., Srayko, M. & Rose, A. M. Mutational analysis of *bli-4/kpc-4* reveals critical
771 residues required for proprotein convertase function in *C. elegans*. *Gene* **252**, 15-25,
772 doi:10.1016/s0378-1119(00)00211-0 (2000).

773 53 Cardoso, J., Felix, R., Fonseca, V. & Power, D. Feeding and the Rhodopsin Family G-
774 Protein Coupled Receptors in Nematodes and Arthropods. *Frontiers in Endocrinology* **3**,
775 doi:10.3389/fendo.2012.00157 (2012).
776 54 Beets, I., Lindemans, M., Janssen, T. & Verleyen, P. Deorphanizing G protein-coupled
777 receptors by a calcium mobilization assay. *Methods Mol Biol* **789**, 377-391,
778 doi:10.1007/978-1-61779-310-3_25 (2011).
779 55 Au, V. *et al.* CRISPR/Cas9 Methodology for the Generation of Knockout Deletions in
780 *Caenorhabditis elegans*. *G3 (Bethesda, Md.)* **9**, 135-144, doi:10.1534/g3.118.200778
781 (2019).
782 56 Bentley, B. *et al.* The Multilayer Connectome of *Caenorhabditis elegans*. *PLoS*
783 *computational biology* **12**, e1005283, doi:10.1371/journal.pcbi.1005283 (2016).
784 57 Gulia-Nuss, M., Robertson, A. E., Brown, M. R. & Strand, M. R. Insulin-like peptides
785 and the target of rapamycin pathway coordinately regulate blood digestion and egg
786 maturation in the mosquito *Aedes aegypti*. *PLoS One* **6**, e20401,
787 doi:10.1371/journal.pone.0020401 (2011).
788 58 Dhara, A. *et al.* Ovary ecdysteroidogenic hormone functions independently of the insulin
789 receptor in the yellow fever mosquito, *Aedes aegypti*. *Insect Biochem Mol Biol* **43**, 1100-
790 1108, doi:10.1016/j.ibmb.2013.09.004 (2013).
791 59 Terrill, S. J. *et al.* Nucleus accumbens melanin-concentrating hormone signaling
792 promotes feeding in a sex-specific manner. *Neuropharmacology* **178**, 108270,
793 doi:10.1016/j.neuropharm.2020.108270 (2020).

60 Tonoki, A., Ogasawara, M., Yu, Z. & Itoh, M. Appetitive Memory with Survival Benefit Is Robust Across Aging in *Drosophila*. *J Neurosci* **40**, 2296-2304, doi:10.1523/jneurosci.2045-19.2020 (2020).

61 Rojo Romanos, T., Petersen, J. G., Riveiro, A. R. & Pocock, R. A novel role for the zinc-finger transcription factor EGL-46 in the differentiation of gas-sensing neurons in *Caenorhabditis elegans*. *Genetics* **199**, 157-163, doi:10.1534/genetics.114.172049 (2015).

62 Chew, Y. L., Grundy, L. J., Brown, A. E. X., Beets, I. & Schafer, W. R. Neuropeptides encoded by *nlp-49* modulate locomotion, arousal and egg-laying behaviours in C*aenorhabditis elegans* via the receptor SEB-3. *Philos Trans R Soc Lond B Biol Sci* **373**, doi:10.1098/rstb.2017.0368 (2018).

63 Fadda, M. *et al.* NPY/NPF-Related Neuropeptide FLP-34 Signals from Serotonergic Neurons to Modulate Aversive Olfactory Learning in *Caenorhabditis elegans*. *The Journal of Neuroscience* **40**, 6018, doi:10.1523/JNEUROSCI.2674-19.2020 (2020).

64 Fadda, M. *et al.* Regulation of Feeding and Metabolism by Neuropeptide F and Short Neuropeptide F in Invertebrates. *Frontiers in endocrinology* **10**, 64-64, doi:10.3389/fendo.2019.00064 (2019).

65 Hobert, O. The neuronal genome of *Caenorhabditis elegans*. *WormBook*, 1-106, doi:10.1895/wormbook.1.161.1 (2013).

66 Nelson, M. D. *et al.* FRPR-4 Is a G-Protein Coupled Neuropeptide Receptor That Regulates Behavioral Quiescence and Posture in *Caenorhabditis elegans*. *PLoS One* **10**, e0142938, doi:10.1371/journal.pone.0142938 (2015).

816 67 Park, D. *et al.* Interaction of structure-specific and promiscuous G-protein-coupled
817 receptors mediates small-molecule signaling in *Caenorhabditis elegans*. *PNAS* **109**,
818 9917-9922, doi:10.1073/pnas.1202216109 (2012).
819 68 Cook, S. J. *et al.* Whole-animal connectomes of both *Caenorhabditis elegans* sexes.
820 *Nature* **571**, 63-71, doi:10.1038/s41586-019-1352-7 (2019).
821 69 Van Sinay, E. *et al.* Evolutionarily conserved TRH neuropeptide pathway regulates
822 growth in *Caenorhabditis elegans*. *Proc Natl Acad Sci U S A* **114**, E4065-e4074,
823 doi:10.1073/pnas.1617392114 (2017).
824 70 Peymen, K. *et al.* Myoinhibitory peptide signaling modulates aversive gustatory learning
825 in *Caenorhabditis elegans*. *PLoS Genet* **15**, e1007945, doi:10.1371/journal.pgen.1007945
826 (2019).

827

828

Acknowledgements

We thank the *Caenorhabditis* Genetics Center, which is funded by the NIH Office of Research Infrastructure Programs (P40 OD01044), as well as Dr. Paul Sternberg (CalTech), Dr. Chris Li (CUNY), the National BioResource Project, Dr. Ding Xue (UC Boulder), and Dr. Maureen Barr (Rutgers) for providing strains. The synthetic ascr#8 utilized in this study was generously provided by Frank Schroeder (Cornell University). We want to thank Dr. Don Moerman (UBC; C. elegans Knockout Facility) for providing the *frpr-16* knockout. We thank InVivo Biosciences for generating transgenic animals by injection. We thank Kate Pearce and Suzanne Scarlatta for assistance in confocal fluorescent imaging the *npr-10* and *frpr-16* reporter strains, as well as Dr. Jeremy Florman of Mark Alkema's lab for assistance in *flp-3* reporter imaging. We also would like to thank Dr. Victor Ambros (UMass Medical School), Dr. Shreekanth Chalasani (Salk Institute), Dr. Josh Hawk (Yale), and Dr. Dominic Esposito (Addgene) for providing us with the necessary plasmid reagents. We acknowledge and thank Profs. Frank Schroeder and Shreekanth Chalasani, as well as members of the Srinivasan lab for their feedback on this manuscript. Funding for this work was provided under the Research foundation Flanders (FWO) project grant G0C0618N (I.B.), and the National Institutes of Health grants R01 NS107475 (M.J.A.), and R01 DC016058-01 (J.S.).

Competing interests

No competing interests are declared.

Author contributions

D.K.R. performed behavioral assays, contributed to the single worm assay design, performed all molecular biology, performed and designed peptide rescue experiments, performed the statistical analyses, and led manuscript writing and revision. E.J.M., H.T.N., and A.N.R contributed to the

852 behavioral assays and as well as manuscript revisions. E.V. and I.B. performed the GPCR
853 activation assays, as well as contributed to manuscript revisions. I.B. also provided funding for
854 the GPCR activation studies. W.J. contributed to injections of the *flp-3* rescue, while M.J.A.
855 provided comments on manuscript. R.J.G. assisted in the development of the single worm assay
856 design, J.S. and D.K.R. wrote the manuscript with input from M.A., R.J.G.

857 **Figure Legends**

858

859 **Figure 1. Attraction to ascr#8 is sex specific. (A)** Design of the Single Worm Attraction Assay
860 (SWAA). The outer 40 wells of a 48-well suspension cell culture plate are seeded with NGM
861 agar and a thin lawn of OP50 *E. coli*. A random block design results in spatial control (light
862 grey), vehicle control (dark grey), and ascaroside (purple) containing wells. Quadrants are
863 recorded for 15 minutes. **(Inset)** The structure of ascr#8. **(B)** Raw dwell times of males of control
864 lines in SWAA. **(C)** Transformed log(fold-change) of male dwell time data. **(D)** Raw dwell time
865 and **(E)** log(fold-change) of hermaphrodites across strains. Light grey denotes spatial controls
866 ("S") (when applicable), dark grey denotes vehicle controls ("V") , colors denote ascr#8 values
867 ("A") (N2, blue; *him-5*, red; *him-8*, purple; *osm-3;him-5*, orange). For all figures: Error bars
868 denote SEM. $n \geq 5$. * $p < 0.05$, ** $p < 0.01$, *** $p < 0.001$, **** $p < 0.0001$, unless denoted
869 otherwise. For **1B**: ++++ $p < 0.0001$, vehicle vs. spatial control.

870

Figure 2. Peptidergic regulation of the male behavioral response to ascr#8. (A, B) A screen of neuropeptide defective mutants. **(A)** Raw dwell time and **(B)** log(fold-change) values. **(C)** Avoidance assay comparing *him-8* and *flp-3* males. **(D)** Hermaphroditic raw dwell time and **(E)** log(fold-change) values in response to ascr#8. **(F)** Hermaphroditic *him-8* and *flp-3* ascr#8 avoidance. **(G-I)** Effect of expressing *flp-3* under its endogenous promoter on both attractive behavior **(G)** raw dwell times and **(H)** log(fold-change) values, as well as **(I)** the avoidance phenotype. **(J-L)** Expression of *pflp-3*::*flp-3*::mCherry within the male tail, co-localizing with *gpa-1*::GFP in the SPD spicule neurons (arrows). * denotes coelomocyte accumulation of GFP. **(J)** GFP, **(K)** mCherry, **(L)** merged image at ~90X magnification. In panel **(H)**, ◊◊, $p < 0.01$ for *flp-3* mutant versus transgenic rescue.

Figure 3. The G protein-coupled Receptor, NPR-10, is required for the male behavioral response to ascr#8. (A) Previously identified FLP-3 peptide affinities for known receptors. Adapted from Li and Kim, 2014 [22]. **(B)** Raw dwell time and **(C)** log(fold-change) values for *npr* receptor mutants and *npr-10* rescue in the SWAA. **(D)** Avoidance indexes of *npr* receptor mutants and rescue. **(E)** Localization of p*npr-10*::*npr-10*::GFP in the amphid region of the male head. Localization includes the inner labial neurons, IL2, and their respective socket cells (ILso), the interneurons RMEV and RMEL, the chemosensory neurons ADL and ASG, as well as the interneurons AVF and AVK. **(F)** Expression of p*npr-10*::*npr-10*::GFP in the mail tail. Localization is observed in the B-class Ray neurons.

Figure. 4. FLP-3 peptides activate the G protein-coupled receptors, NPR-10 and FRPR-16, *in vitro*. Dose response curves of **(A)** FLP-3-1, **(B)** FLP-3-2, **(C)** FLP-3-3, **(D)** FLP-3-4, **(E)** FLP-3-5, **(F)** FLP-3-7, **(G)** FLP-3-8, **(H)** and FLP-3-9 for activation of NPR-10B (blue circles) and FRPR-16 (red triangles). Peptides FLP-3-6 and FLP-3-10 did not activate either receptor. **(I)** EC_{50} values and 95% Confidence Intervals for FLP-3 peptide activating NPR-10B and FRPR-16. **(A-H**) Error bars denote SEM. $n \geq 6$.

Figure 5. FRPR-16 is required for the male behavioral response to ascr#8. (A, B) Design of CRISPR/Cas9-mediated *frpr-16* null mutation. **(A)** The wild-type gene, with CRISPR cut sites marked, along with 450 bp homology arm regions. **(B)** The mutant gene sequence, consisting of an inverted cassette driving loxP flanked p*myo-2*::GFP and p*rps-27*::neoR expression. **(C)** Raw dwell time and **(D)** log(fold-change) values for *frpr-16 lof* animals, transgenic rescues, and *frpr-16;npr-10* double mutant animals. **(E)** Avoidance indexes of *frpr-16 lof* animals, transgenic rescues, and *frpr-16;npr-10* double mutant animals. **(F)** Expression of p*frpr-16*::*frpr-16*::SL2::mCherry in male *C. elegans* at 20X magnification. Localization within the ventral cord denoted. **(F, inset)**, Amphid localization of p*frpr-16*::*frpr-16*::SL2::mCherry at ~120X within the reverse locomotion command interneurons, AVA, AVE, and AVD, as well as the BAG neuron (anterior to the nerve ring). In panel **(D)** ◊◊, $p < 0.01$ for *frpr-16 lof* mutant versus transgenic rescue.

Figure 6. Peptide feeding rescues wild-type behavior and reveals two active peptides within the FLP-3 precursor. (A) Overview of rescue-by-feeding paradigm. **(Top)** the peptide of interest is flanked by EGL-3 cleavage sites, with a 6x-His tag upstream. **(Bottom)** *flp-3 lof* animals are raised on bacteria expressing a FLP-3 peptide of interest and are assayed as young adults. **(B)** Avoidance indexes of *him-8* and *flp-3* animals raised on scramble, FLP-3-1, FLP-3-2, FLP-3-4, FLP-3-9, and FLP-3-10 peptides. **(C)** Raw dwell time and **(D)** log(fold-change) values for *him-8* and *flp-3* animals raised on scramble, FLP-3-2, and FLP-3-9 peptides. Active peptides shown in pink.

Figure 7. Two FLP-3 NP/NPR modules mediate the male behavioral response to ascr#8. The neuropeptide gene *flp-3* is expressed in the IL1 neurons in the head and the SPD spicule neurons in the tail (teal). Following release of processed FLP-3 peptides, FLP-3-2 and FLP-3-9 are sensed by NPR-10 and FRPR-16 expressing neurons (blue and red, respectively) to mediate dwelling in the mating pheromone by modulating forward and reverse locomotion. Green neurons are connections inferred from the male synaptic connectome [68]. Gold denotes the command interneuron AVB and the forward locomotory circuitry.

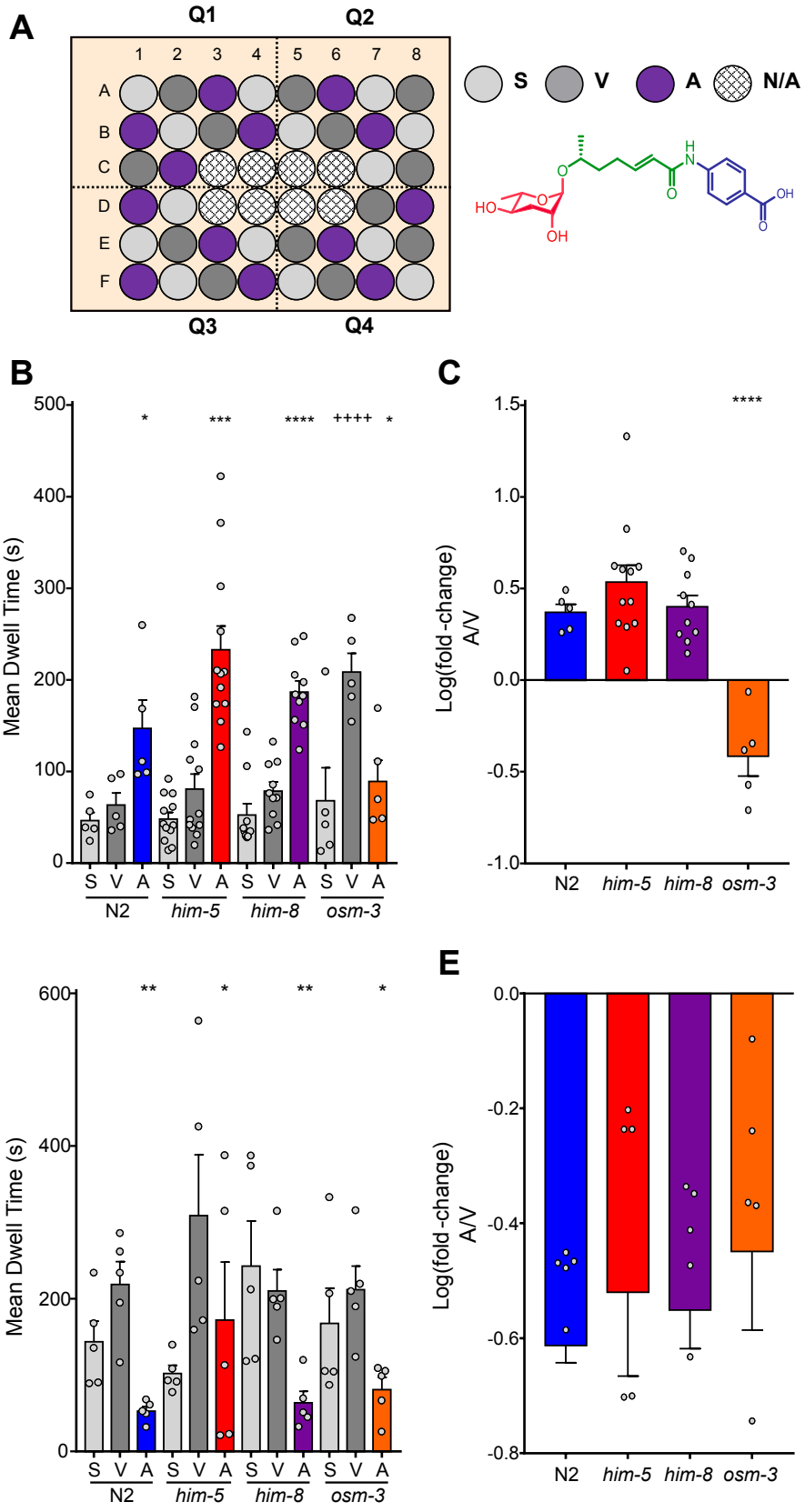

Figure-1

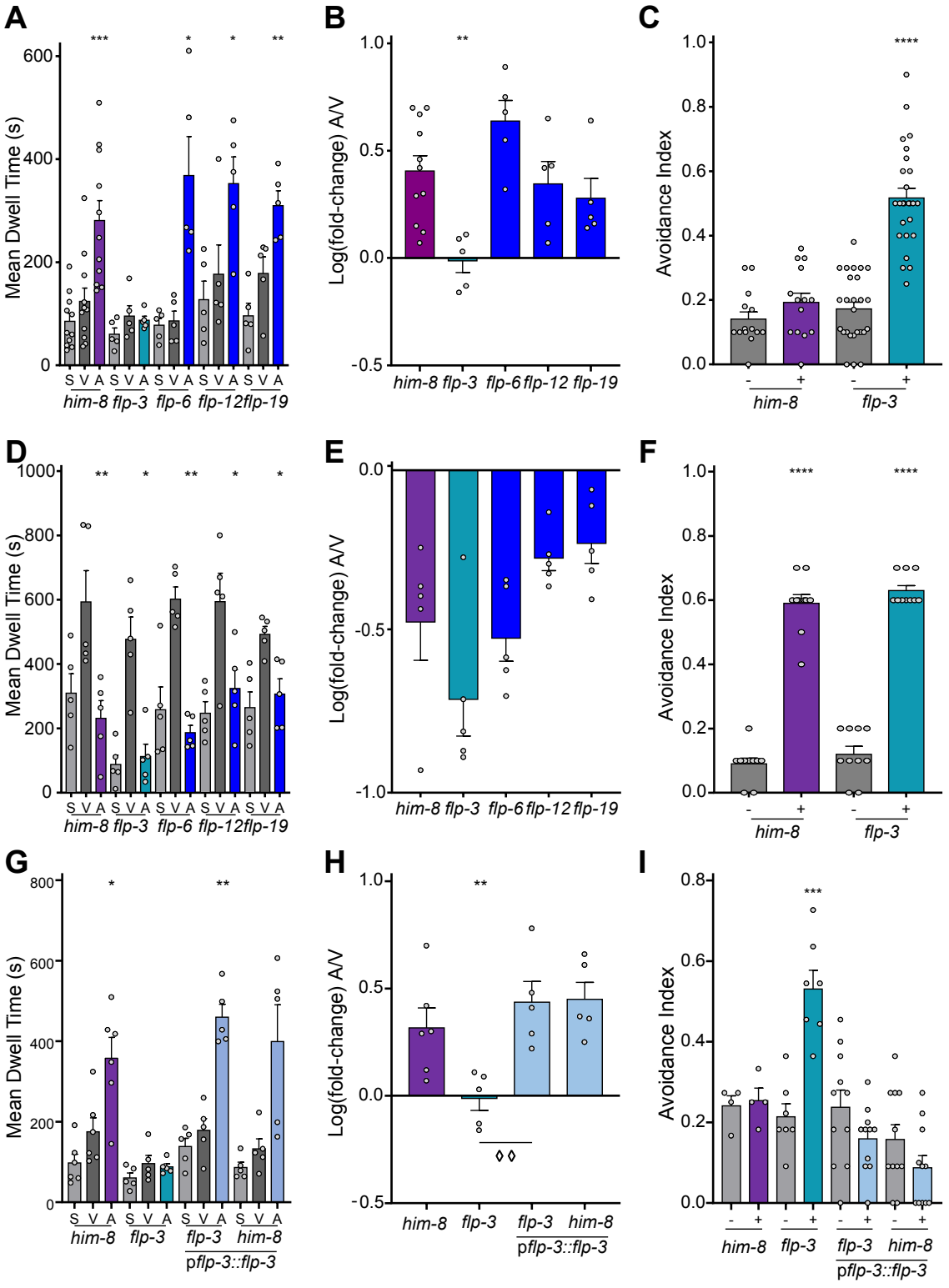

Figure-2

A

	FLP-3 Peptide	Receptor		
		npr-4	*npr-5*	*npr-10*
		C16D6.2	Y58G8A.4	C53C7.1
3-1	SPLGTMRFamide	mM	mM	nM
3-2	TPLGTMRFamide			
3-3	EAEEPLGTMRFamide			nM
3-4	NPLGTMRFamide			
3-5	ASEDALFGTMRFamide			nM
3-6	EDGNAPFGTMKFamide		mM	nM
3-7	SAEPFGTMRFamide	mM	mM	nM
3-8	SADDSAPFGTMRFamide		mM	nM
3-9	NPENDTPFGTMRFamide			
3-10	STVDSSEPVIRDQ			

B

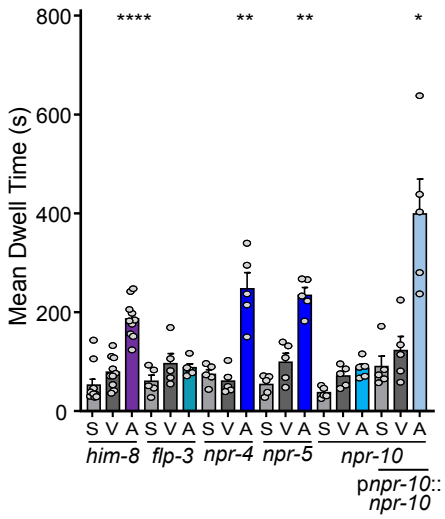

C

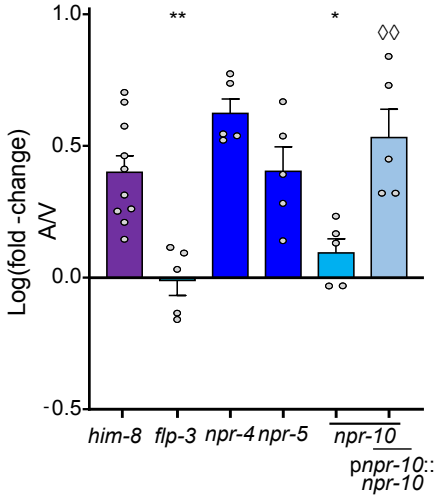

D

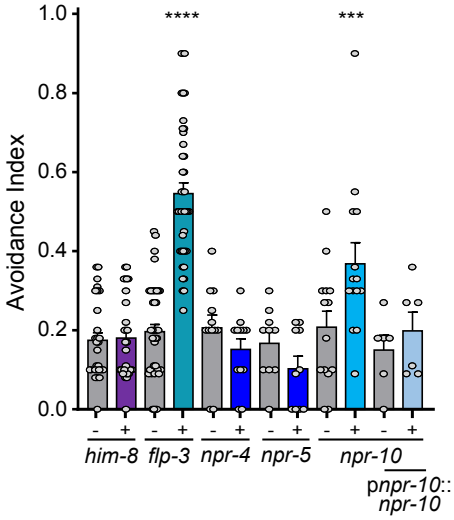

E

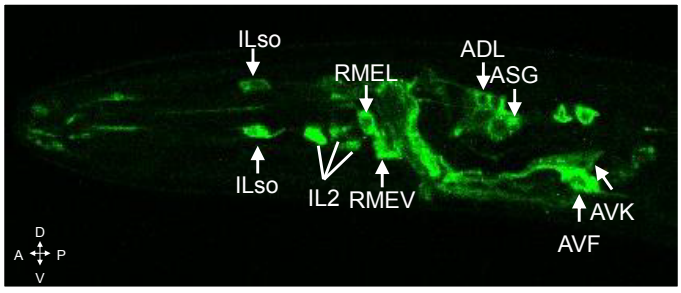

F

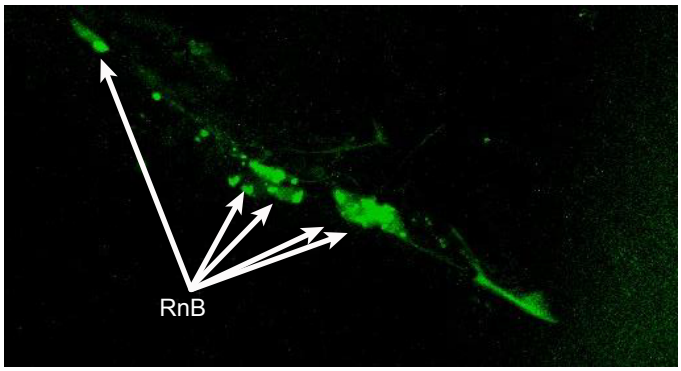

Figure-3

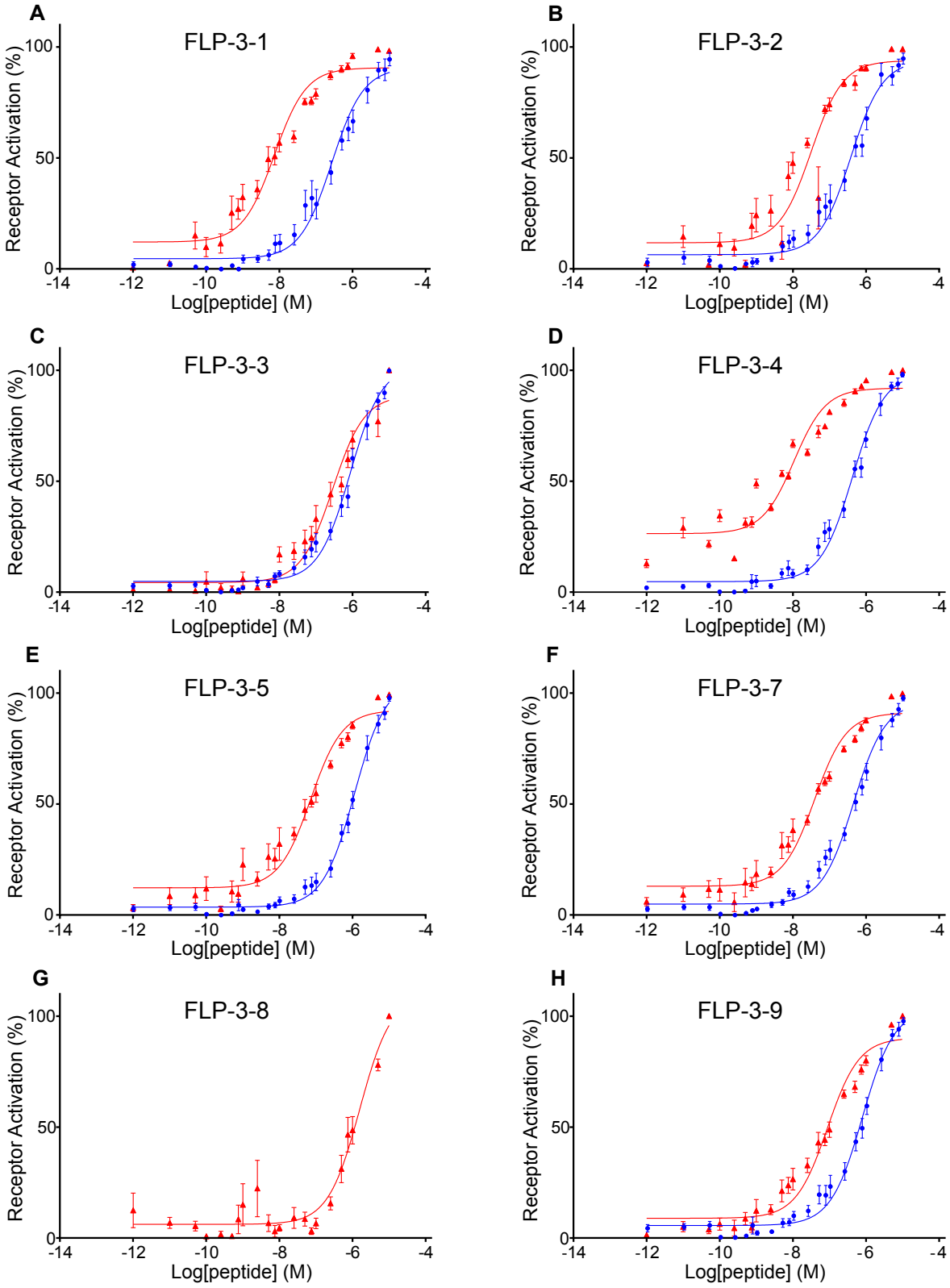

I

		NPR-10		FRPR-16	
	FLP-3 Peptide	EC_{50}	95% CI	EC_{50}	95% CI
3-1	SPLGTMRFamide	262.1 nM	189.7 nM to 359.8 nM	7.4 nM	5.2 nM to 10.6 nM
3-2	TPLGTMRFamide	366.5 nM	270.4 nM to 491.3 nM	31.7 nM	19.0 nM to 51.2 nM
3-3	EAEEPLGTMRFamide	866.7 nM	706.6 nM to 1.1 µM	288.3 nM	203.7 nM to 402.3 nM
3-4	NPLGTMRFamide	427.1 nM	351.7 nM to 516.3 nM	10.7 nM	7.6 nM to 15.3 nM
3-5	ASEDALFGTMRFamide	1.1 µM	946.2 nM to 1.4 µM	72.1 nM	51.1 nM to 101.3 nM
3-7	SAEPFGTMRFamide	438.6 nM	351.3 nM to 530.1 nM	39.5 nM	28.5 nM to 54.0 nM
3-8	SADDSAPFGTMRFamide	N/A	N/A	1.6 µM	1.1 µM to 2.4 µM
3-9	NPENDTPFGTMRFamide	760.1 nM	624.1 nM to 923.3 nM	88.3 nM	65.2 nM to 119.6 nM

Figure-4

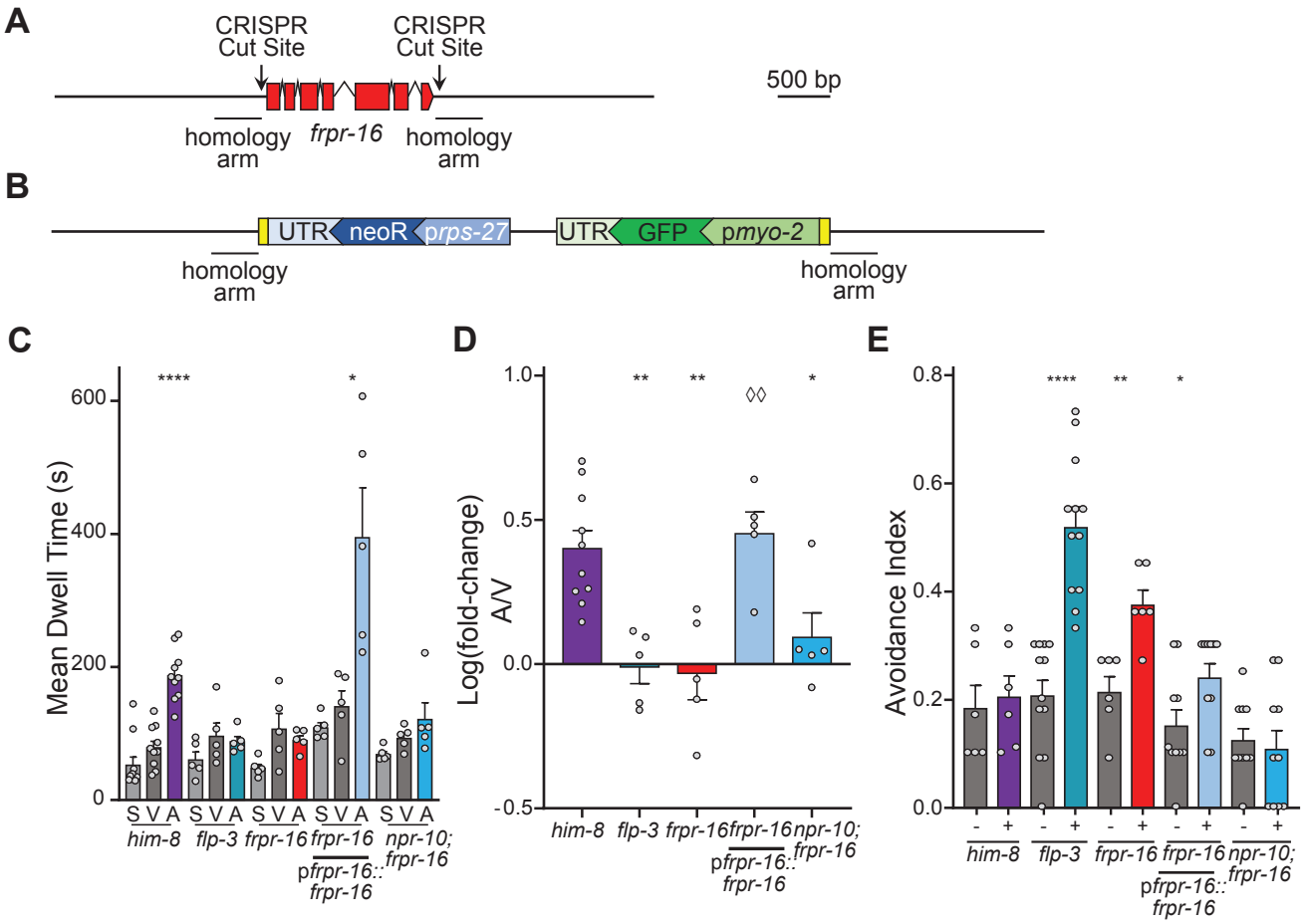

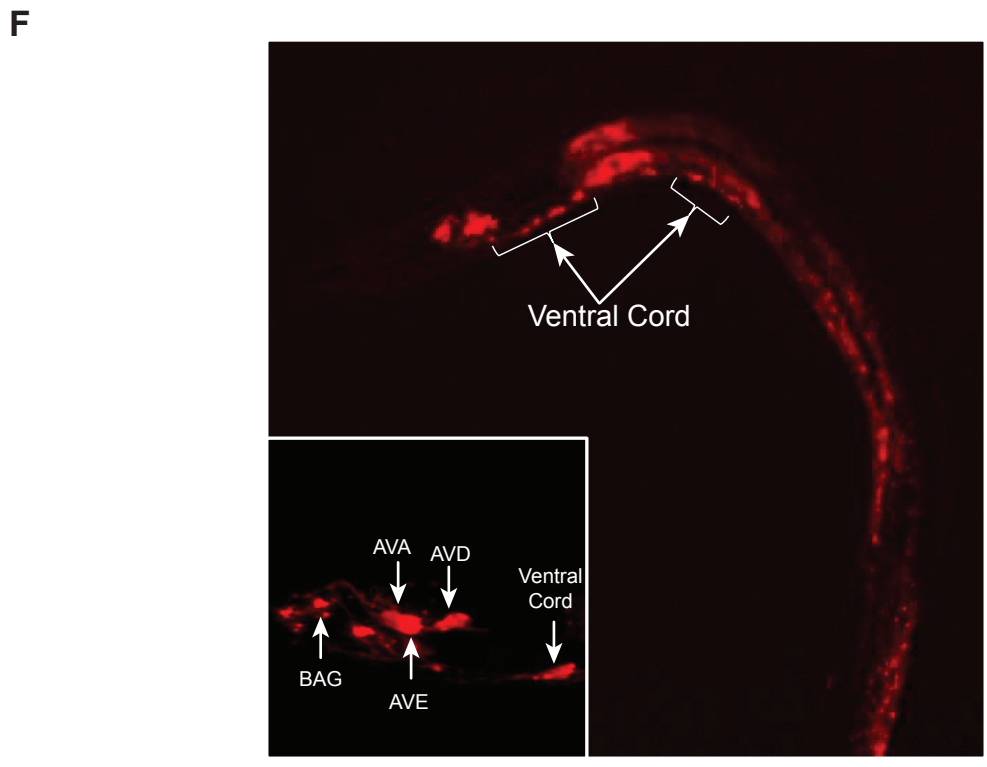

Figure-5

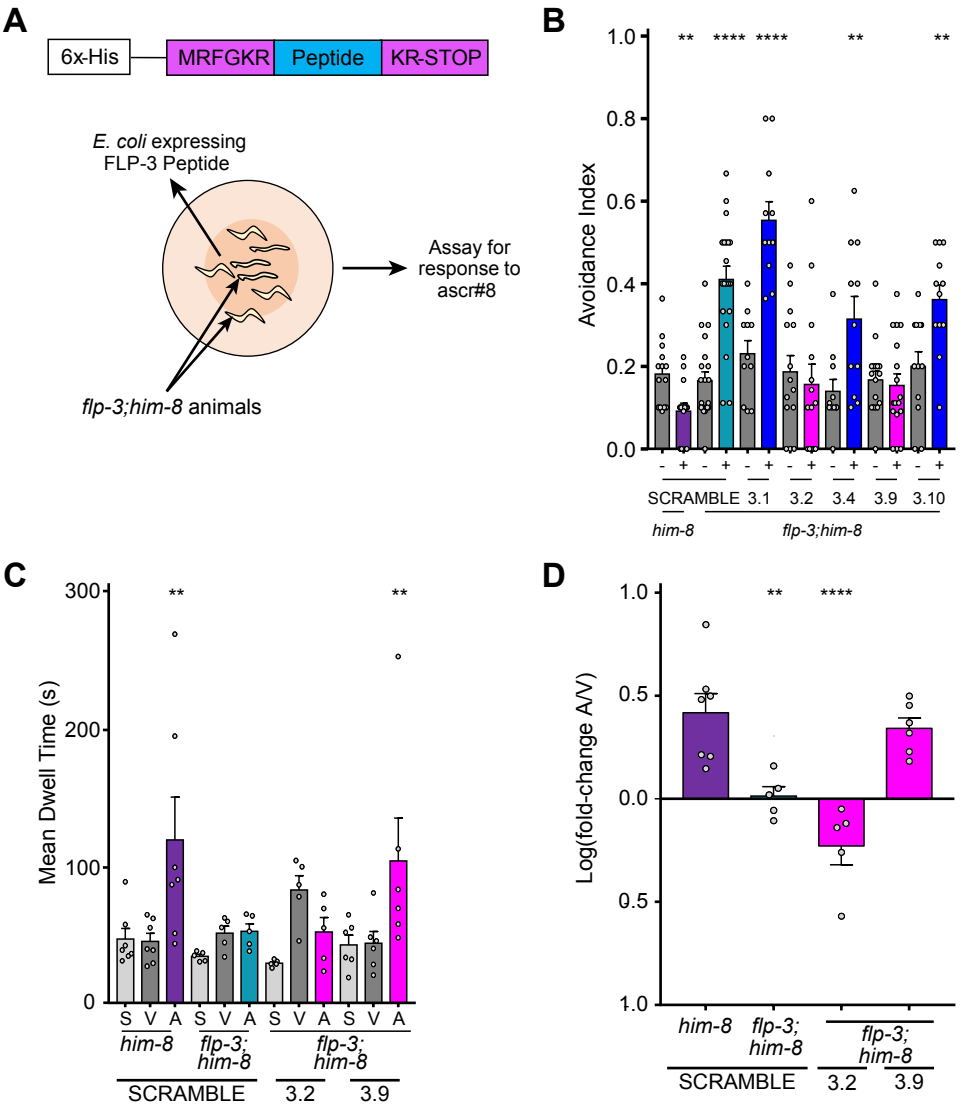

Figure-6

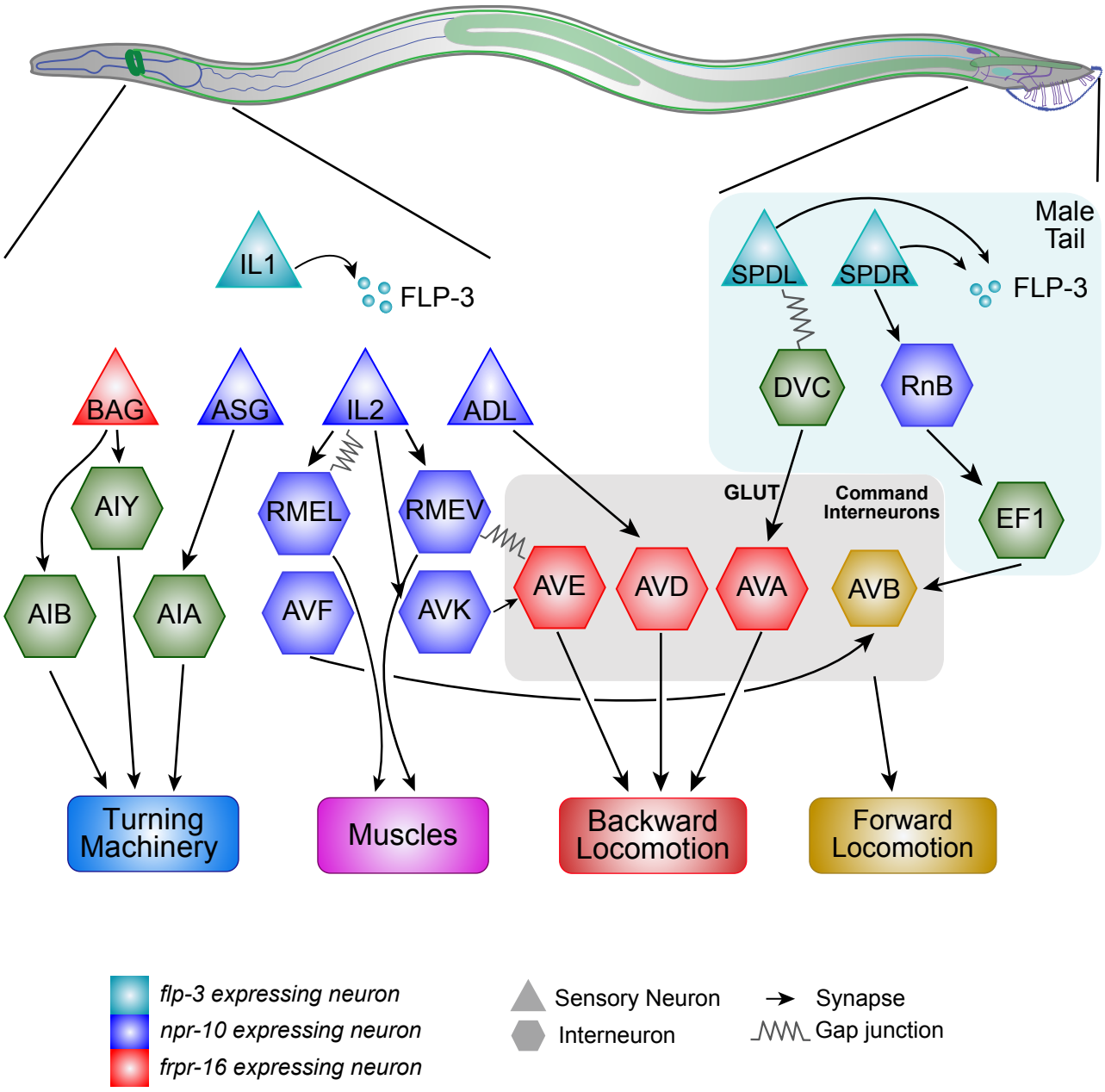

Figure-7